Benchmark Calculations on the Electron Detachment Energies of MO_3^- and $M_2O_6^-$ (M = Cr, Mo, W)

Shenggang Li and David A. Dixon*

*Chemistry Department, The University of Alabama, Shelby Hall, Box 870336,
Tuscaloosa, Alabama 35487-0336*

Received: June 19, 2007; In Final Form: August 14, 2007

Neutral and anionic molecules of the monomers and dimers of the group VIB transition metal oxides (MO_3 and M_2O_6) were studied with density functional theory (DFT) and coupled cluster CCSD(T) theory. Franck−Condon simulations of the photoelectron spectra were carried out for the transition from the ground state of the anion to that of the neutral molecule. Molecular structures from the DFT and CCSD(T) methods are compared. Electron detachment energies reported in the literature were evaluated. The calculated adiabatic and vertical electron detachment energies (ADEs and VDEs) were compared with the experimental results. CCSD(T) gives results within 0.12 eV for the ADEs. CCSD(T) predicts VDEs that are in error by as much as 0.3 eV for M = Cr. DFT hybrid functionals were found to give poor results for the ADEs and VDEs for M = Cr due to the substantial amount of multireference character in the wavefunction, whereas the pure DFT functionals give superior results. For M = Mo and W, excellent agreement was found for both CCSD(T) and many DFT fucntionals. The BP86 functional yields the best overall results for the VDEs of all the metal oxide clusters considered. Heats of formation calculated at the CCSD(T) level extrapolated to the complete basis set limit are also in good agreement with available experimental data.

Introduction

Supported or unsupported transition metal oxides (TMOs) have been used as catalysts for a number of industrial processes due to their rich chemistry. TMO clusters serve as models of catalysts and, in some cases, as the actual catalysts, for example, the polyoxometalates.[1] Experimental methods, especially spectroscopic methods, have been widely used to study clusters of various sizes. When the experimental work is combined with results from electronic structure calculations, significant insight into their electronic properties can be gained. However, the study of large TMO clusters poses significant challenges to both experimental and computational methods. For example, in gas-phase photodetachment experiments, larger clusters require superior mass resolution with a higher detection limit and may be prone to dissociation. In addition, there are also synthetic issues in terms of controlling the cluster size so as to obtain unique clusters in sufficient quantities. Computationally, the potential energy surfaces can be more complicated for larger numbers of atoms and the larger size demands substantially more computing resources.

Traditionally, transition metal compounds can be difficult to treat computationally due to the presence of low-lying electronic states and substantial electron correlation effects. Accurate results can usually be obtained only with high-level correlation methods, which are applicable to relatively small molecules. Density functional theory (DFT)[2] is often the method of choice because it does provide a reasonable treatment of the electronic properties of many transition metal compounds.[3,4] One of the difficulties with the application of DFT methods is that different exchange−correlation functionals can give rather different results and there is no means to know *a priori* which functional performs the best without fairly thorough benchmarking. Although the performance of the various functionals for the properties of the main group element compounds is fairly well studied, there were fewer benchmark studies for transition metal compounds because of the lack of experimental and/or high-level calculations.

Benchmarking of DFT for transition metal compounds that compare the performance of different functionals has recently been carried out by Truhlar and co-workers[5,6] and Furche and Perdew,[7] among others. The former evaluated the performance of various functionals in terms of metal−metal bond energies and bond lengths,[5] as well as reaction energies.[6] They found that the BLYP functional[8,9] gives the best results for the bond energies.[5] The latter investigated the performance of different functionals for the calculations of bond energies, structures, dipole moments, and harmonic frequencies and found that the BP86[8,10] and TPSS[11] functionals have the best price to performance ratio.

In this report, we benchmarked the performance of a wide range of DFT exchange−correlation functionals, as well as the coupled cluster method at the CCSD(T) (couple cluster with single and double excitations and an approximate triples correction) level, for the calculations of the electron detachment energies of anionic group VIB TMO clusters.[12−15] The calculations were carried out for the $(MO_3)_n$ (M = Cr, Mo, W; $n = 1$, 2) clusters and their anions to obtain the adiabatic and vertical electron detachment energies (ADEs and VDEs) for the anions. The purpose of our study was 2-fold: (1) we want to better understand the experimental data, and (2) we want to determine the performance of various functionals and the accuracy of the CCSD(T) method for these properties. The results from our study can then be applied to the studies of larger TMO clusters. We have previously reported DFT calculations of the properties of the transition metal oxide clusters $(MO_3)_n$ for $n = 1$ to 6 and for M = Cr, Mo, and W.[16]

---

* Corresponding author. E-mail: dadixon@bama.ua.edu.

10.1021/jp074768i CCC: $37.00

TABLE 1: Benchmarked DFT Exchange−Correlation Functionals

method	exchange functional	correlation functional	type[a]	ref
SVWN5	Slater	VWN functional V	LSDA	18,19
BLYP	Becke 88	Lee−Yang−Parr	GGA	8, 9
BP86	Becke 88	Perdew 86	GGA	8, 10
BPW91	Becke 88	Perdew−Wang 91	GGA	8, 20
BB95	Becke 88	Becke 95	GGA	8, 21
PW91	Perdew−Wang 91	Perdew−Wang 91	GGA	22, 20
mPWPW91	Barone's modified PW91	Perdew−Wang 91	GGA	23, 20
PBE	Perdew−Burke−Ernzerhof	Perdew−Burke−Ernzerhof	GGA	24, 25
OLYP	Handy's OPTX	Lee−Yang−Parr	GGA	26, 9
TPSS	Tao−Perdew−Staroverov−Scuseria	Tao−Perdew−Staroverov−Scuseria	GGA	11
VSXC	van Voorhis−Scuseria	van Voorhis−Scuseria	GGA	27
HCTH	Handy's	Handy's	GGA	28, 29, 30
B3LYP	Becke 93	Lee−Yang−Parr	HGGA	17
B3P86	Becke 93	Perdew 86	HGGA	17
B3PW91	Becke 93	Perdew−Wang 91	HGGA	17
B1B95	Becke 96	Becke 95	HGGA	21
B1LYP	Becke 96	Lee−Yang−Parr	HGGA	31
mPW1PW91	Barone's modified PW91	Perdew−Wang 91	HGGA	31
B98	Becke 98	Becke 98	HGGA	32
B971	Handy−Tozer's modified B97	Handy−Tozer's modified B97	HGGA	33
B972	Wilson−Bradley−Tozer's modified B97	Wilson−Bradley−Tozer's modified B97	HGGA	34
PBE1PBE	Perdew−Burke−Ernzerhof	Perdew−Burke−Ernzerhof	HGGA	24
O3LYP	Handy's OPTX	Lee−Yang−Parr	HGGA	35
TPSSh[b]	Tao−Perdew−Staroverov−Scuseria	Tao−Perdew−Staroverov−Scuseria	HGGA	11
BMK	Boese−Martin	Boese−Martin	HGGA	36

[a] LSDA: local spin density approximation. GGA: generalized gradient approximation. HGGA: hybrid GGA. [b] The TPSSh method can be accessed via the option IOp(3/76=0900001000) along with the TPSSTPSS keyword in Gaussian 03.

Computational Methods

Geometries were optimized and harmonic frequencies were calculated at the DFT level with the B3LYP[17] and BP86 functionals. The B3LYP geometries were subsequently used in the single point energy calculations with the other functionals. We employed a wide range of functionals with and without components of Hartree−Fock exchange to benchmark them for use in predicting electron detachment energies for TMO clusters. We used the following functionals (see Table 1): (1) local spin density approximation (LSDA) SVWN5;[18,19] (2) generalized gradient approximations (GGAs) BLYP,[8,9] BP86,[8,10] BPW91,[8,20] BB95,[8,21] PW91,[20,22] mPWPW91,[20,23] PBE,[24,25] OLYP,[9,26] TPSS,[11] and VSXC,[27] and the Handy family of functionals HCTH93, HCTH147, and HCTH407;[28−30] and (3) hybrid GGAs B3LYP, B3P86, B3PW91,[17] B1B95,[21] B1LYP, mPW1PW91,[31] B98,[32] B971,[33] B972,[34] PBE1PBE,[24] O3LYP,[35] TPSSh,[11] and BMK.[36]

We optimized the geometries at the CCSD(T) level.[37−40] For the monomers, we also calculated the harmonic frequencies at the CCSD(T) level. For the dimers, the geometries at the B3LYP level were also employed to calculate the CCSD(T) energies.

We used the augmented correlation-consistent double-ζ (aug-cc-pVDZ) basis set for O[41] and the aug-cc-pVDZ-PP effective core potential (ECP) basis sets for Cr, Mo, and W[42] in the B3LYP and BP86 optimization and frequency calculations; these basis sets are collectively denoted as aD. Single point DFT energy calculations were performed with the aug-cc-pVTZ basis set for O[41] and the aug-cc-pVTZ-PP basis sets for Cr, Mo, and W;[42] these basis sets will be denoted as aT.

The CCSD(T) calculations were performed with the sequence aug-cc-pVnZ for O[41] and aug-cc-pVnZ-PP for Cr, Mo, and W,[42] for n = D, T, Q, with the geometries optimized for n = D and T. The geometries were also optimized at the CCSD(T) level with the aug-cc-pVTZ basis set on O and the ECP10MDF, ECP28MWB, and ECP60MWB basis sets for Cr, Mo, and W, respectively,[43,44] augmented with two sets of f functions and one set of g function as recommended by Martin and Sundermann.[45] These basis sets will be collectively denoted as aT-ECP. For the monomers, harmonic frequencies were also calculated for n = T. The CCSD(T) energies were extrapolated to the complete basis set (CBS) limit by fitting to a mixed Gaussian/exponential formula.[46] The cardinal numbers for the aD, aT, and aQ basis sets depend on the value of $l_{\max}$ as discussed below. Core−valence (CV) correlation corrections were calculated at the CCSD(T) level with the aug-cc-pwCVnZ basis set for O[47,48] and the aug-cc-pwCVnZ-PP basis sets for Cr, Mo, and W,[42] with n = D and T. In addition, relativistic corrections were calculated as expectation values of the mass−velocity and Darwin terms (MVD) from the CISD (configuration interaction with single and double excitations) wavefunction with the aT basis set. A potential problem arises in computing the scalar relativistic correction for the molecules in this study as there is the possibility of "double counting" the relativistic effect on the metal when applying a MVD correction to an energy that already includes some relativistic effects via the relativistic ECP. Because the MVD operators mainly sample the core region where the pseudo-orbitals are small, we assume any double counting to be small. The above approach follows on ours and others' work on the accurate prediction of the heats of formation for a wide range of compounds.[49−65]

All of the DFT calculations were carried with the Gaussian 03 program package.[66] For the pure DFT methods, the density fitting approximation was employed to speed up the calculations.[67,68] The density fitting sets were automatically generated from the atomic orbital primitives.

The CCSD(T) calculations were carried out with the MOLPRO 2006.1[69] and the NWChem 5.0 program packages.[70,71] The open-shell calculations were done with the R/UCCSD(T) approach where a restricted open shell Hartree−Fock (ROHF) calculation was initially performed and the spin constraint was then relaxed in the coupled cluster calculation.[72−74] We note that the calculated (T) contributions are slightly different in the MOLPRO and NWChem implementations for R/UCCSD(T).

The calculations were carried out on the Opteron-based Cray XD1 and Itanium 2-based SGI Altix supercomputers at the

Alabama Supercomputer Center, the Xeon-based Dell Linux cluster at the University of Alabama, the local Opteron-based Parallel Quantum Solutions Linux cluster, and the Itanium 2-based Linux cluster at the Molecular Science Computing Facility from the Pacific Northwest National Laboratory.

Multidimensional Franck−Condon factors for the vibronic transitions from the ground state of the anion to that of the neutral cluster were calculated within the harmonic approximation to simulate the photoelectron spectrum. The program[75] was adapted from the work of Yang et al.[76] and the algorithms from Gruner and Brumer,[77] Ruhoff and Ratner,[78] and Hazra and Nooijen.[79] The B3LYP and BP86 equilibrium geometries, as well as their harmonic frequencies and normal coordinates were used in these simulations. A Boltzmann distribution was used to account for the finite temperature effect with a Lorentzian line shape.

Atomization energies of the M_nO_{3n} ($n = 1, 2$) clusters at 0 K were calculated as the energy differences between the ground states of the atoms and those of the clusters following our previous work in the references given above:

$$\Sigma D_{0,0K} = \Delta E_{CBS} + \Delta E_{ZPE} + \Delta E_{CV} + \Delta E_{SR} + \Delta E_{SO} \qquad (1)$$

where

$$\Delta E = nE(M,{}^7S_3) + 3nE(O,{}^3P_2) - E(M_nO_{3n}) \qquad (2)$$

We chose to use the $^7S_3$ state of the metal, as it is the ground state for Cr and Mo and the lowest excited state for W. The $^7S_3$ state has no atomic spin orbit correction, and it is not necessary to deal with averaging of orbital configurations. For W, the atomic ground state is the $^5D_0$ state with a large spin orbit correction and we corrected the calculated energy difference using eq 2 with the experimental energy difference between the $^5D_0$ and $^7S_3$ states (8.43 kcal/mol).[80] The spin−orbit contribution for O is 0.223 kcal/mol. For the B3LYP, BP86, and PW91 methods, eq 1 reduces to

$$\Sigma D_{0,0K} = \Delta E_e + \Delta E_{ZPE} + \Delta E_{SO} \qquad (3)$$

Heats of formation of the clusters at 0 K are calculated from the atomization energies and the experimental heats of formation for the atoms:[81]

$$\Delta H_{f,0K}(M_nO_{3n}) = n\Delta H_{f,0K}(M) + 3n\Delta H_{f,0K}(O) - \Sigma D_{0,0K}(M_nO_{3n}) \qquad (4)$$

The heats of formation at 0 K for the elements in the gas phase are $\Delta H_f^0(O) = 58.98 \pm 0.02$ kcal mol^{-1}, $\Delta H_f^0(Cr) = 94.5 \pm 1.0$ kcal mol^{-1}, $\Delta H_f^0(Mo) = 157.1 \pm 0.9$ kcal mol^{-1}, and $\Delta H_f^0(W) = 203.1 \pm 1.5$ kcal mol^{-1}. Heats of formation at 298 K are calculated by following the procedures outlined by Curtiss et al.[82]

Results and Discussion

MO_3. Table 2 lists the bond length, bond angle, and pyramidal angle (for a molecule XY_3 with C_{3v} symmetry, the pyramidal angle is defined as the angle between the X−Y bond and the C_3 axis; for a planar D_{3h} molecule, this angle is 90°) optimized at the B3LYP and CCSD(T) levels for the ground states of MO_3 and MO_3^- (M = Cr, Mo, W) as shown schematically in Figure 1. All molecules were predicted to be pyramidal in their ground states except for CrO_3^-, which was predicted to be planar. The O═M═O bond angle decreases with increasing atomic number of the metal atom; i.e., the molecule becomes more pyramidal.

TABLE 2: Optimized Bond Lengths (Å) and Bond Angles (deg) for the Ground States of MO_3 and MO_3^- (M = Cr, Mo, W) at the B3LYP and CCSD(T) Levels

	CrO_3	CrO_3^-	MoO_3	MoO_3^-	WO_3	WO_3^-
			M═O			
B3LYP/aD	1.578	1.623	1.713	1.752	1.725	1.761
CCSD(T)/aD	1.600	1.639	1.730	1.766	1.742	1.774
CCSD(T)/aT	1.596	1.637	1.719	1.753	1.732	1.763
CCSD(T)/aT-ECP	1.592	1.633	1.715	1.750	1.737	1.768
			∠O═M═O			
B3LYP/aD	115.1	120.0	110.9	117.0	108.0	116.1
CCSD(T)/aD	115.7	120.0	111.0	117.5	108.5	116.1
CCSD(T)/aT	115.1	120.0	110.9	116.9	108.4	115.9
CCSD(T)/aT-ECP	114.2	120.0	108.0	116.9	108.3	115.9
			Pyramidal Angle[a]			
B3LYP/aD	103.0	90.0	108.0	100.0	110.9	101.5
CCSD(T)/aD	102.1	90.0	107.9	99.2	110.4	101.5
CCSD(T)/aT	103.0	90.0	108.0	100.3	110.6	101.8
CCSD(T)/aT-ECP	104.2	90.0	110.9	100.3	110.6	101.8

[a] The angle between the C_3 axis and the X−Y bond in XY_3.

The calculated pyramidal angle is about 10° smaller for the anion than the neutral for M = Mo and W and about 5° smaller for M = Cr. The fact that CrO_3^- is planar is not surprising, as the neutral is almost planar and the pyramidal angle decreases as an electron is added. The CCSD(T)/aD bond length is only slightly longer than the CCSD(T)/aT value for M = Cr and is about 0.01 Å longer for M = Mo and W. The CCSD(T)/aT-ECP value is slightly shorter than the CCSD(T)/aT value for M = Cr and Mo, but slightly longer for M = W. The B3LYP/aD bond length is about 0.02 Å shorter than the CCSD(T)/aT result for M = Cr, and slightly shorter for M = Mo and slightly longer for M = W. Most of the calculated angles at the different computational levels are the same within 1°.

The photoelectron spectrum of CrO_3^- obtained at 266 nm displays a relatively short vibrational progression with a spacing of ∼890 (60) cm^{-1}, which was assigned to the Cr═O symmetric stretching vibration.[12] We predict this stretching frequency to be 873 and 947 cm^{-1} at the BP86/aD and CCSD(T)/aT levels, which agree with the experimental value within its large uncertainty. At the B3LYP/aD level, this stretching frequency was calculated to be 1012 cm^{-1}; the substantial overestimate is consistent with the fact that this method yields a much shorter Cr═O bond length than the CCSD(T)/aT method. Gutsev et al.[12] used the BPW91 method and obtained a value of 960 cm^{-1} for this frequency, in better agreement with the experimental result than the B3LYP method. The reason for the superior performance of the BP86 and BPW91 method will be discussed in more detail below. Furthermore, there are weak bands to the red of these vibrational bands. On the basis of the spectra, both the adiabatic and vertical electron detachment energies (ADEs and VDEs) were originally reported as 3.66 (2) eV.[12] The spectrum has because been reinterpreted to assign the VDE to be 3.77 eV.[83]

To determine the correctness of the above assignments, we carried out Franck−Condon simulations for the electronic transitions from the ground state of the anion to that of the neutral molecule using the B3LYp/aD and BP86/aD optimized geometries and Cartesian harmonic force constants, which are shown in Figure 1a. For the symmetric stretch to have the dominant intensity, as observed in the experimental spectrum, it is necessary for the neutral molecule to be planar or much closer to planar and that the short progression be due to a low inversion barrier. The $^1A_1$ state undergoes vertex inversion through a planar CrO_3 transition state ($^1A_1'$) with one imaginary frequency (156i, 193i, and 150i cm^{-1} at the B3LYP/aD, BP86/

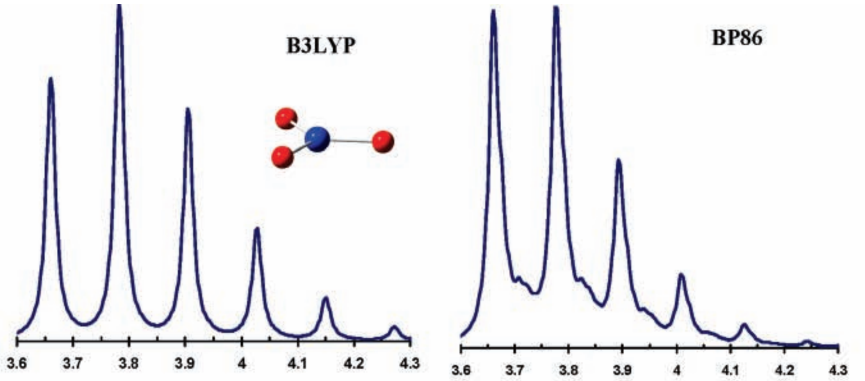

(a) CrO_3^-, ${}^1A_1' \leftarrow {}^2A_1'$

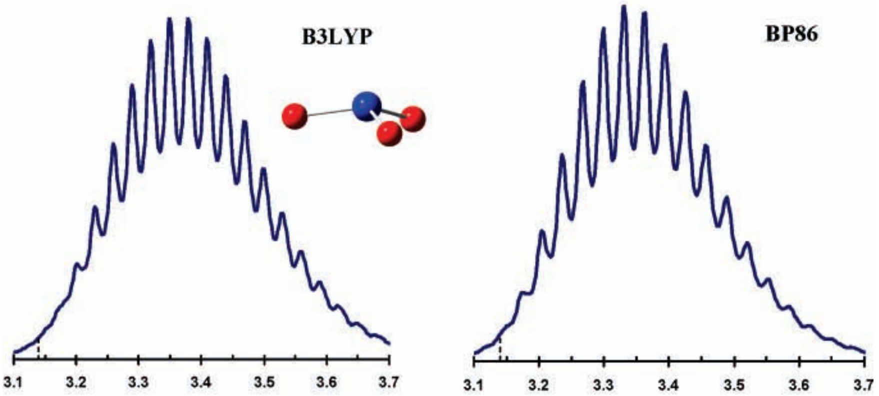

(b) MoO_3^-, ${}^1A_1 \leftarrow {}^2A_1$

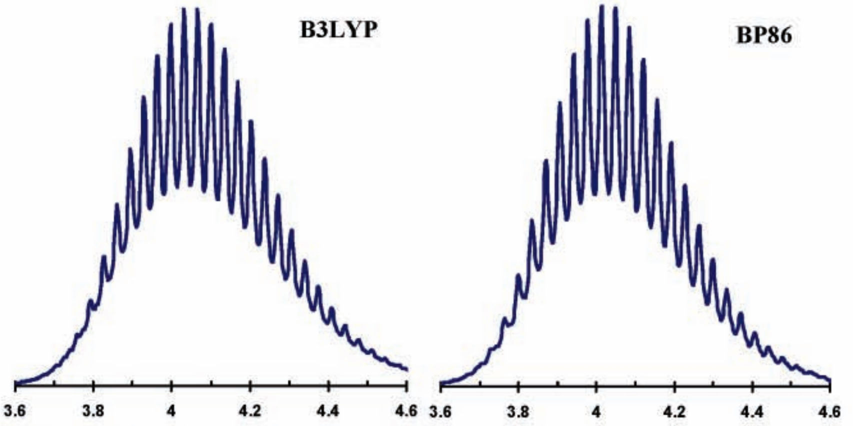

(c) WO_3^-, ${}^1A_1 \leftarrow {}^2A_1$

Figure 1. Franck−Condon simulations of the photoelectron spectra of MO_3^- at the B3LYP/aD and BP86/aD levels: (a) CrO_3^-, ${}^1A_1' \leftarrow {}^2A_1'$ (planar); (b) MoO_3^-, ${}^1A_1 \leftarrow {}^2A_1$ (pyramidal); (c) WO_3^-, ${}^1A_1 \leftarrow {}^2A_1$ (pyramidal). The full width at half-maximum (FWHM) is 20 meV, and the vibrational temperature is 100 K.

aD, and CCSD(T)/aT levels, respectively). The transition state lies only 1.3, 3.0, and 1.5 kcal/mol at the B3LYP/aD, BP86/aD, and CCSD(T)/CBBBS levels, respectively, higher in energy than the ${}^1A_1$ state. The electronic barrier heights are 1.6, 3.4, and 1.8 kcal/mol when the zero-point vibrational energies (ZPEs) are excluded. The simulations for the $X'({}^1A_1') \leftarrow X({}^2A_1')$ transition at the B3LYP/aD and BP86/aD levels are shown in Figure 1a, with a 0−0 transition energy of 3.66 eV and the imaginary frequency of its absolute value. They display the expected short progression and are close to the experimental spectrum with the BP86/aD spectrum closer to experiment. The inversion vibration is inactive, because it is not totally symmetric in D_{3h} symmetry as it is in C_{3v} symmetry. The simulated progression is assigned to the Cr═O symmetric stretching vibration. Overall, the vertical transition produces the most favorable Franck−Condon factor for the CrO_3^-/CrO_3 system to which the strongest band is assigned. The fact that the first two bands have similar intensity makes it difficult to decide which one should be assigned to the VDE. The calculations show that the second band is slightly more intense and is best assigned to the VDE.

The ground states of both MoO_3 and WO_3 and their anions were predicted to be pyramidal at the B3LYP, BP86, and CCSD(T) levels. The photoelectron spectra reported by Wang and co-workers for these anions display broad peaks for the transitions to the ground state of the neutral molecules.[13] The spectrum for MoO_3^- at 355 nm exhibits a long vibrational progression with a spacing of 230 (30) cm^{-1}. The spectrum for

TABLE 3: Adiabatic and Vertical Electron Detachment Energies (ADEs/VDEs, eV) for the Ground State of MO_3^- (M = Cr, Mo, W) Calculated at the CCSD(T) Level and Compared with the Experimental Values

	ΔE_{aD}	ΔE_{aT}	ΔE_{aQ}	ΔE_{CBS}[a]	ΔE_{ZPE}[b]	ΔE_{CV}[c]	ΔE_{SR}[d]	$\Delta E_{\mathrm{total}}$[e]	expt.
					ADEs				
CrO_3^-	3.651	3.680	3.692	3.699	+0.030	+0.060 (+0.057)	−0.005	3.78	3.66(2)[f]
MoO_3^-	3.078	3.062	3.070	3.074	+0.028	+0.086 (+0.101)	−0.005	3.18	3.14(2)[g]
WO_3^-	3.399	3.407	3.422	3.430	+0.019	+0.049 (+0.064)	−0.004	3.50	3.62(5)[g]
					VDEs				
CrO_3^-	3.801	3.854	3.888	3.909		+0.078 (+0.057)	−0.005	3.98	3.77(2)[f]
MoO_3^-	3.302	3.265	3.291	3.307		+0.118 (+0.106)	−0.004	3.42	3.33(5)[g]
WO_3^-	3.707	3.704	3.730	3.745		+0.106 (+0.095)	−0.004	3.85	3.83(3)[g]

[a] Extrapolated using the mixed Gaussian/exponential formula (ref 46) for the CCSD(T) energies with the aD, aT, and aQ basis sets. In comparison, the ADEs are calculated to be 3.686, 3.044, and 3.370 eV, and the VDEs are calculated to be 3.893, 3.248, and 3.672 eV for M = Cr, Mo, and W, respectively with the aT-ECP basis sets. [b] CCSD(T)/aT. [c] CCSD(T)/aug-cc-pwCVTZ/aug-cc-pwCVTZ-PP. The CCSD(T)/aug-cc-pwCVDZ/aug-cc-pwCVDZ-PP results are shown in the parentheses. [d] CISD/aT. [e] $\Delta E_{\mathrm{total}} = \Delta E_{\mathrm{CBS}} + \Delta E_{\mathrm{ZPE}} + \Delta E_{\mathrm{CV}} + \Delta E_{\mathrm{SR}}$. [f] References 12 and 83. See text. [g] Reference 13.

WO_3^- recorded by Stolcic et al. at 4.66 eV displays a similar long vibrational progression with a spacing of ~240 cm^{-1}.[84] The frequency of the inversion vibration was calculated to be 241, 257, and 239 cm^{-1} at the B3LYP/aD, BP86/aD, and CCSD(T)/aT levels for MoO_3 and 277, 288, and 263 cm^{-1} for WO_3, consistent with the experimental values. The simulated spectra from the B3LYP/aD and BP86/aD calculations are shown in Figure 1b for M = Mo, and in Figure 1c for M = W. All simulated spectra are dominated by the inversion vibration. The strongest band in the simulated spectra is the seventh band for M = Mo and the 13th band for M = W, whereas it is ≥fourth for M = Mo and ≥sixth for M = W in the experimental spectra. Due to the large displacement along the inversion vibrational mode resulting from the large difference in the pyramidal angle, the 0−0 transition has a negligible Franck−Condon factor. This means that there will be a large uncertainty in the measured ADE, whereas the experimental VDE will be more accurate. Similar to the planar CrO_3, planar MO_3 for M = Mo and W are also transition states with imaginary frequencies of 193i and 192i cm^{-1} at the B3LYP/aD and CCSD(T)/aT levels for M = Mo and 232i and 231i cm^{-1} for M = W. However, the barrier for vertex inversion in MoO_3 and WO_3 was predicted to be much larger than that for CrO_3. At the B3LYP/aD and CCSD(T)/CBS levels, the inversion barrier was calculated to be 6.4 and 7.0 kcal/mol for M = Mo and 15.0 and 15.6 kcal/mol for M = W. The planar transition state for MO_3^- has a smaller imaginary frequency, 102i and 99i cm^{-1} at the B3LYP/aD and CCSD(T)/aT levels for M = Mo and 107i and 113i cm^{-1} for M = W. The inversion barriers in the anions are small, 0.4 and 0.6 kcal/mol for M = Mo and 0.9 and 1.0 kcal/mol for M = W at the B3LYP/aD and CCSD(T)/CBS levels, respectively. The simulation for the transition from the planar anion to the pyramidal neutral molecule results in a longer progression due to the larger difference in the pyramidal angles.

Table 3 lists the calculated ADEs and VDEs with the CCSD(T) method and compares them with the experimental values. The basis set, core−valence, and scalar relativistic contributions are listed separately to allow for the assessment of the individual effects, as well as the vibrational ZPE contribution to the ADEs. The conclusions from these results are valuable for the calculations for larger systems when large basis set or core−valence calculations are intractable. We compare the VDEs first, as they are the more accurate experimental quantities especially for MoO_3^- and WO_3^-. The best estimated CCSD(T) value is 0.21 eV higher than the experimental value for CrO_3. This discrepancy is much smaller for MoO_3 (0.09 eV), and negligible for WO_3 (0.02 eV). Considering that the experimental uncertainties for the VDEs of MoO_3^- and WO_3^- are likely to be somewhat larger than those reported by Wang and co-workers,[12] the CCSD(T) method essentially reproduces the experimental measurements. However, the VDE of CrO_3^- is slightly overestimated by the CCSD(T) method. This may be attributed to the multireference character of the wavefunction for M = Cr. The T_1 diagnostic[85] for the $^1A_1$ state of CrO_3 from the CCSD(T) calculations is about 0.055 when the frozen-core approximation is applied and 0.045 otherwise. The T_1 diagnostic for the $^2A_1'$ state ranges from 0.040 to 0.050. The $^1A_1'$ transition state at the anion geometry required for the calculation of the VDE has a slightly larger T_1 diagnostic than those for the $^1A_1$ state. In contrast, the T_1 diagnostics are significantly smaller for M = Mo and W, ranging from 0.030 to 0.040 and 0.025 to 0.035, respectively. In addition, the basis set effect for the calculated VDEs is slightly different for M = Cr than for M = Mo and W. The CCSD(T)/CBS value is larger than the CCSD(T)/aD value by 0.11 eV for M = Cr, whereas this difference is much smaller for M = Mo and W, 0.01 and 0.04 eV, respectively. The CCSD(T)/aT-ECP results are thus in reasonable agreement with the CCSD(T)/CBS values due to the relatively small basis set effect. The core−valence effect causes the VDE to further increase and is smaller for M = Cr (0.08 eV) than for M = Mo and W (0.12 and 0.11 eV), whereas the scalar relativistic effect slightly reduces the VDE by <0.01 eV. The negligible scalar relativistic effect is consistent with the use of the relativistic ECP for the metal atoms and the fact that we are not dramatically changing the electronic structure on removal of an electron from the anion to form the neutral.

Similar conclusions can be made for the calculated ADEs. The ADE at the CCSD(T)/CBS level is larger than the experimental value by 0.12 eV for M = Cr, is smaller by 0.12 eV for M = W, and is larger by 0.04 eV as compared to the experimental value for M = Mo. Considering the uncertainties associated with the experimental values, this is very good agreement. The basis set effect on the ADE is slightly smaller than that for the VDE for M = Cr, whereas it is comparable for M = Mo and W. The core−valence effect to the ADE is smaller than that for the VDE, whereas the scalar relativistic effect is also negligible. As the core−valence effect appears to be comparable to the basis set effect for M = Cr and significantly larger for M = Mo and W, we also calculated ΔE_{CV} with the smaller aug-cc-pwCVDZ and aug-cc-pwCVDZ-PP basis sets. The core−valence contributions from these calculations recover most of those calculated with the larger basis sets.

One potential alternative to the CCSD(T) approach to improve the agreement between theory and experiment for the VDE and ADE of CrO_3 is to use renormalized CCSD(T) theory at the completely renormalized (CR)[86] or locally renormalized (LR)[87] CCSD(T) levels where the latter is based on the numerator−denominator-connected expansion.[88] We performed calculations

TABLE 4: Adiabatic and Vertical Electron Detachment Energies (ADEs/VDEs, eV) for the Ground State of MO_3^- (M = Cr, Mo, W) Calculated with Various Exchange−Correlation Functionals and the aT Basis Sets at the B3LYP/aD Geometries and Compared with the CCSD(T) and Experimental Values[a]

	ADE			VDE		
functional	CrO_3^-	MoO_3^-	WO_3^-	CrO_3^-	MoO_3^-	WO_3^-
B3LYP[b]	4.06 (+0.40)	3.30 (+0.16)	3.55 (−0.07)	4.27 (+0.50)	3.53 (+0.20)	3.93 (+0.10)
B3P86	4.49 (+0.83)	3.75 (+0.61)	4.03 (+0.41)	4.79 (+1.02)	4.07 (+0.74)	4.48 (+0.65)
B3PW91	3.92 (+0.26)	3.18 (+0.04)	3.46 (−0.16)	4.20 (+0.43)	3.49 (+0.16)	3.90 (+0.07)
B1B95	3.85 (+0.19)	3.05 (−0.09)	3.32 (−0.30)	4.16 (+0.39)	3.38 (+0.05)	3.76 (−0.07)
B1LYP	4.05 (+0.39)	3.21 (+0.07)	3.48 (−0.14)	4.27 (+0.50)	3.46 (+0.13)	3.84 (+0.01)
mPW1PW91	4.02 (+0.36)	3.22 (+0.08)	3.50 (−0.12)	4.33 (+0.56)	3.54 (+0.21)	3.94 (+0.11)
B98	3.92 (+0.26)	3.09 (−0.05)	3.35 (−0.27)	4.19 (+0.42)	3.37 (+0.04)	3.76 (−0.07)
B971	3.85 (+0.19)	3.02 (−0.12)	3.26 (−0.36)	4.09 (+0.32)	3.29 (−0.04)	3.67 (−0.16)
B972	3.65 (−0.01)	2.88 (−0.26)	3.16 (−0.46)	3.95 (+0.18)	3.21 (−0.12)	3.61 (−0.22)
PBE1PBE	3.97 (+0.31)	3.17 (+0.03)	3.45 (−0.17)	4.28 (+0.51)	3.51 (+0.18)	3.90 (+0.07)
O3LYP	3.52 (−0.14)	2.86 (−0.28)	3.14 (−0.48)	3.74 (−0.03)	3.17 (−0.16)	3.60 (−0.23)
TPSSh	3.69 (+0.03)	3.02 (−0.12)	3.30 (−0.32)	3.90 (+0.13)	3.27 (−0.06)	3.71 (−0.12)
BMK	5.05 (+1.39)	3.55 (+0.41)	3.66 (+0.04)	5.37 (+1.60)	3.81 (+0.48)	4.00 (+0.17)
SVWN5	3.46 (−0.20)	3.01 (−0.13)	3.23 (−0.39)	3.78 (+0.01)	3.39 (+0.06)	3.82 (−0.01)
BLYP	3.52 (−0.14)	2.96 (−0.18)	3.18 (−0.44)	3.58 (−0.19)	3.12 (−0.21)	3.56 (−0.27)
BP86	3.60 (−0.06)	3.07 (−0.07)	3.33 (−0.29)	3.74 (−0.03)	3.32 (−0.01)	3.77 (−0.06)
BPW91	3.46 (−0.20)	2.92 (−0.22)	3.18 (−0.44)	3.60 (−0.17)	3.17 (−0.16)	3.63 (−0.20)
BB95	3.26 (−0.40)	2.76 (−0.38)	2.99 (−0.63)	3.39 (−0.38)	3.00 (−0.33)	3.44 (−0.39)
PW91	3.53 (−0.13)	2.99 (−0.15)	3.25 (−0.37)	3.69 (−0.08)	3.25 (−0.08)	3.71 (−0.12)
mPWPW91	3.50 (−0.16)	2.96 (−0.18)	3.22 (−0.40)	3.65 (−0.12)	3.21 (−0.12)	3.67 (−0.16)
PBE	3.45 (−0.21)	2.92 (−0.22)	3.17 (−0.45)	3.59 (−0.18)	3.17 (−0.16)	3.64 (−0.19)
OLYP	3.17 (−0.49)	2.63 (−0.51)	2.90 (−0.72)	3.32 (−0.45)	2.90 (−0.43)	3.37 (−0.46)
TPSS	3.48 (−0.18)	2.92 (−0.22)	3.19 (−0.43)	3.62 (−0.15)	3.16 (−0.17)	3.60 (−0.23)
VSXC	3.47 (−0.19)	2.86 (−0.28)	3.13 (−0.49)	3.68 (−0.09)	3.11 (−0.22)	3.55 (−0.28)
HCTH93	3.20 (−0.46)	2.67 (−0.47)	2.96 (−0.66)	3.40 (−0.37)	2.98 (−0.35)	3.44 (−0.39)
HCTH147	3.38 (−0.28)	2.84 (−0.30)	3.11 (−0.51)	3.57 (−0.20)	3.14 (−0.19)	3.60 (−0.23)
HCTH407	3.44 (−0.22)	2.90 (−0.24)	3.17 (−0.45)	3.63 (−0.14)	3.21 (−0.12)	3.66 (−0.17)
CCSD(T)	3.78 (+0.12)	3.18 (+0.04)	3.50 (−0.12)	3.98 (+0.21)	3.42 (+0.09)	3.85 (+0.02)
expt	3.66 ± 0.05	3.14 ± 0.02	3.62 ± 0.05	3.77 ± 0.05	3.33 ± 0.05	3.83 ± 0.03

[a] The difference between the calculated and the experimental values is shown in the parentheses. [b] At the B3LYP/aD level, the ADEs are calculated to be 4.06, 3.33, and 3.57 eV, and the VDEs are calculated to be 4.26, 3.53, and 3.91 eV for M = Cr, Mo, and W, respectively.

at the CR and LR levels with the aD basis set for CrO_3 and CrO_3^- at the optimized CCSD(T)/aD geometries. At the LR-CCSD(T) level, we used the six different three-body corrections to the CCSD energies given by Kowalski.[86] The energy results are given in the Supporting Information. The CR calculations led to increases in the VDE and ADE of 0.10−0.25 eV as did the IB, IIB, and IIIB LR approximations. Thus these approaches lead to larger discrepancies with experiment as compared to CCSD(T). The results at the level of LR-CCSD(T) with the IA, IIA, and IIIA approximations lead to a decrease in the VDE of 0.09−0.12 eV, resulting in better agreement with experiment. For the ADE, the decrease ranges from 0.04 eV at the LR-CCSD(T),IA level to 0.14 eV at the LR-CCSD(T),IIIA level. The LR-CCSD(T) methods can slightly improve the calculated values for the electron detachment energies for the chromium species by about 0.05−0.10 eV but we have no *a priori* way for picking the best LR approximation. In addition, we performed complete active space self-consistent field (CASSCF) calculations on CrO_3 and CrO_3^- with the aD basis set. We kept the O(2s) electrons frozen so there were 18 active electrons in 15 orbitals (O(2p), Cr(3d,4s)). The calculated valence electronic component of the VDE at the CASSCF level is only 1.48 eV and that of the ADE is 1.35 eV. The CASSCF values are more than 2 eV below the CCSD(T)/aD result or the experimental value showing the need for additional correlation.

Table 4 compares the experimental and calculated ADEs and VDEs from the various DFT functionals at the B3LYP/aD geometries. In terms of the VDEs, the B3LYP functional significantly overestimates the VDE by 0.50 eV for M = Cr, but yields fairly good VDEs for M = Mo and W within 0.2 eV. This is consistent with the performance of the CCSD(T) method discussed above. The multireference character is significant for M = Cr, resulting in the poor performance of the B3LYP functional due to its inclusion of a component of Hartree−Fock (HF) exchange. This is also consistent with the calculated VDEs from the other hybrid DFT functionals. For M = Cr, most of the hybrid functionals yield VDEs more than 0.4 eV higher than the experimental value. The exceptions are the B971, B972, and TPSSh functionals, which give values 0.32, 0.18, and 0.13 eV higher, respectively, and the O3LYP functional, which gives a value 0.03 eV lower. In contrast, most of the pure DFT functionals gives VDEs within 0.2 eV of the experimental values, with the exceptions of the BB95, OLYP, and HCTH93 functionals, which give values 0.38, 0.45, and 0.37 eV lower, respectively, than the experimental value.

For M = Mo, most of the hybrid functionals and the majority of the pure functionals yield VDEs within 0.2 eV from the experimental value, but significantly fewer functionals give VDEs within 0.1 eV. The B1B95, B98, B971, TPSSh, SVWN5, BP86, and PW91 functionals give values within 0.1 eV. The B3P86 and BMK functionals substantially overestimate the VDE by more than 0.5 eV, whereas the BB95, OLYP, and HCTH93 functionals significantly underestimate the VDE by more than 0.3 eV. The B3P86 method has been shown to overestimate the adiabatic ionization potentials for a number of metal complexes.[89−92]

For M = W, majority of the hybrid functionals yield VDEs within 0.1 eV from the experimental value, whereas only a few pure functionals give VDEs within 0.1 eV. The B971, B972, O3LYP, and BMK hybrid functionals overestimate the VDE by about 0.2 eV, whereas the B3P86 overestimates it by about 0.7 eV. Among the pure functionals, only the SVWN5 and BP86 functionals give VDEs within 0.1 eV, and most of them

TABLE 5: Optimized Bond Lengths (Å) and Bond Angles (deg) for the Ground States of M_2O_6 and $M_2O_6^-$ (M = Cr, Mo, W) at the B3LYP and CCSD(T) Levels

	Cr_2O_6	$Cr_2O_6^-$		Mo_2O_6	$Mo_2O_6^-$		W_2O_6	$W_2O_6^-$	
	^1A_g	$^2A_1$	^2A_g	^1A_g	$^2A_1$	^2A_g	^1A_g	$^2A_1$	^2A_g
				M═O					
B3LYP/aD	1.558	1.586/1.591	1.587	1.692	1.723/1.723	1.723	1.710	1.734/1.735	1.735
CCSD(T)/aD	1.574	1.598/1.606	1.600	1.705	1.734/1.735	1.735	1.722	1.745/1.748	1.747
CCSD(T)/aT	1.572		1.598	1.694		1.724	1.713		1.737
CCSD(T)/aT-ECP	1.567		1.593	1.691		1.721	1.719		1.743
				M─O					
B3LYP/aD	1.775	1.724/1.884	1.794	1.925	1.893/2.011	1.948	1.931	1.934/1.978	1.955
CCSD(T)/aD	1.788	1.738/1.896	1.807	1.936	1.886/2.047	1.958	1.943	1.898/2.051	1.967
CCSD(T)/aT	1.782		1.801	1.923		1.946	1.930		1.955
CCSD(T)/aT-ECP	1.779		1.798	1.921		1.943	1.936		1.961
				∠O═M═O					
B3LYP/aD	111.0	110.6/116.9	113.2	109.9	110.9/114.4	112.7	110.4	111.6/112.1	111.9
CCSD(T)/aD	111.2	110.9/116.3	113.6	109.8	110.6/114.9	112.9	110.4	111.1/112.7	112.0
CCSD(T)/aT	111.1		113.6	109.7		112.8	110.4		112.1
CCSD(T)/aT-ECP	111.1		113.5	109.9		112.7	110.3		112.0
				∠O─M─O					
B3LYP/aD	86.6	83.4/93.3	90.6	83.0	83.1/89.6	87.2	82.9	83.7/86.0	84.9
CCSD(T)/aD	87.4	84.4/94.3	91.0	83.7	81.9/90.7	87.8	83.5	80.9/89.0	85.6
CCSD(T)/aT	87.3		91.0	83.4		87.7	83.1		85.4
CCSD(T)/aT-ECP	87.3		90.9	83.4		87.7	82.9		85.2

overestimate the VDE by about 0.3 eV. In terms of the ADEs, similar conclusions can be drawn.

M_2O_6. Table 5 lists the optimized bond lengths and bond angles at the B3LYP and CCSD(T) levels for M_2O_6 and $M_2O_6^-$ (M = Cr, Mo, W) with the structure shown schematically in Figure 2. The ground state of M_2O_6 was predicted by the B3LYP method to be the ^1A_g state in D_{2h} symmetry, whereas the ground state of $M_2O_6^-$ was predicted to be the $^2A_1$ state in C_{2v} symmetry. The ^2A_g state of $M_2O_6^-$ was predicted to have one imaginary frequency, 793i, 233i, and 141i cm^{-1} for M = Cr, Mo, and W, respectively, at the B3LYP/aD level. The ^2A_g state of the anion lies slightly higher in energy than the $^2A_1$ state for M = Cr by 2.2 kcal/mol (2.9 kcal/mol without the ZPE correction). The ^2A_g state is essentially isoenergetic to the $^2A_1$ state of the anion for M = Mo and W. The energy difference is ~0.2 kcal/mol for M = Mo and ~0.03 kcal/mol for M = W with small differences due to whether the ZPE correction is included.

At the BP86/aD level, the ^2A_g state of the anion was predicted to be the ground state of $M_2O_6^-$ for all three metals and no lower energy structures were found by lowering the symmetry.

We optimized both the $^2A_1$ and ^2A_g states for $M_2O_6^-$ at the CCSD(T)/aD level. Without the ZPE correction, the $^2A_1$ state is ~0.3, ~0.1, and ~0.05 kcal/mol lower in energy than the ^2A_g state for M = Cr, Mo, and W, respectively. Therefore, both states are likely to be present and it is not possible yet to computationally predict which is the ground state of the anion.

For the ^1A_g of the neutral and ^2A_g states of the anion, the M═O and M─O bond lengths optimized at the CCSD(T)/aD level are slightly longer than those at the CCSD(T)/aT level for M = Cr, and they are about 0.01 Å longer than the latter for M = Mo and W. The bond lengths at the CCSD(T)/aT-ECP level are slightly shorter than those at the CCSD(T)/aT level for M = Cr and Mo, but they are slightly longer for M = W. The calculated bond lengths with the B3LYP/aD method are shorter than those at the CCSD(T)/aT level by about 0.01 Å for M = Cr, whereas they are essentially identical for M = Mo and W. Similar behavior was observed for the monomers. The calculated bond angles agree with each other within 1°. For the $^2A_1$ state, the metal−oxygen bond lengths from the B3LYP/aD method are about 0.01 Å shorter than those at the CCSD(T)/aD level for the M═O (M = Cr, Mo, W) and Cr─O bonds. For the Mo─O and W─O bonds, the CCSD(T)/aD method predicted a larger variation than the B3LYP/aD method.

Anionic photoelectron spectra have been reported for $W_2O_6^-$[14] and $Cr_2O_6^-$[15]. For $W_2O_6^-$, partially resolved vibrational structures were observed by Wang and co-workers from the photoelectron spectrum recorded at 266 nm. Three vibrational bands were identified, with the second being the strongest. The simulated spectrum for the $^1A_g \leftarrow {}^2A_1$ transition at the B3LYP/aD level shown in Figure 2a is broader than those for the $^1A_g \leftarrow {}^2A_g$ transition at the B3LYP/aD and BP86/aD levels shown in Figure 2b. The 0−0 transition, whose energy was set to 3.52 eV, has the largest intensity in all of these simulations. However, several bands at ~3.65 eV combine to yield a comparable intensity to that of the 0−0 band. These bands are assigned to the M─O and M═O symmetric stretching vibrations, which are calculated to be 706 and 1035 cm^{-1} by B3LYP/aD and 678 and 995 cm^{-1} by BP86/aD. The experimental spacing of 920 (40) cm^{-1} is comparable to the calculated M═O symmetric stretching frequencies. In addition, the M─O asymmetric stretch leading to the distortion from D_{2h} to C_{2v} symmetry (691 and 670 cm^{-1} from B3LYP/aD and BP86/aD) also has a fairly large Franck−Condon factor in the simulated spectrum for the $^1A_g \leftarrow {}^2A_1$ transition. However, as in the above energetic argument, we cannot exclude either transition from contributing to the experimental spectrum for this molecule.

The simulated spectra for M = Mo and Cr are shown in Figure 2c−f. The 0−0 transition is much weaker in these spectra, indicating larger geometric changes upon electron detachment.

The photoelectron spectrum reported by Wang and co-workers for $Cr_2O_6^-$ was recorded at 266 nm, which also shows a partially resolved vibrational progression with a spacing of 780 cm^{-1}. The simulated spectrum for the $^1A_g \leftarrow {}^2A_1$ transition shown in Figure 2e with the B3LYP/aD method is dominated by the M─O asymmetric stretching vibrations (741 and 711 cm^{-1} from B3LYP/aD and BP86/aD). It does not appear to agree with the experimental spectrum, although this might be due to the B3LYP method itself. For the $^1A_g \leftarrow {}^2A_g$ simulations in Figure 2f, three symmetric vibrations show considerable intensities: the O─M─O bend, M─O and M═O stretches. Their

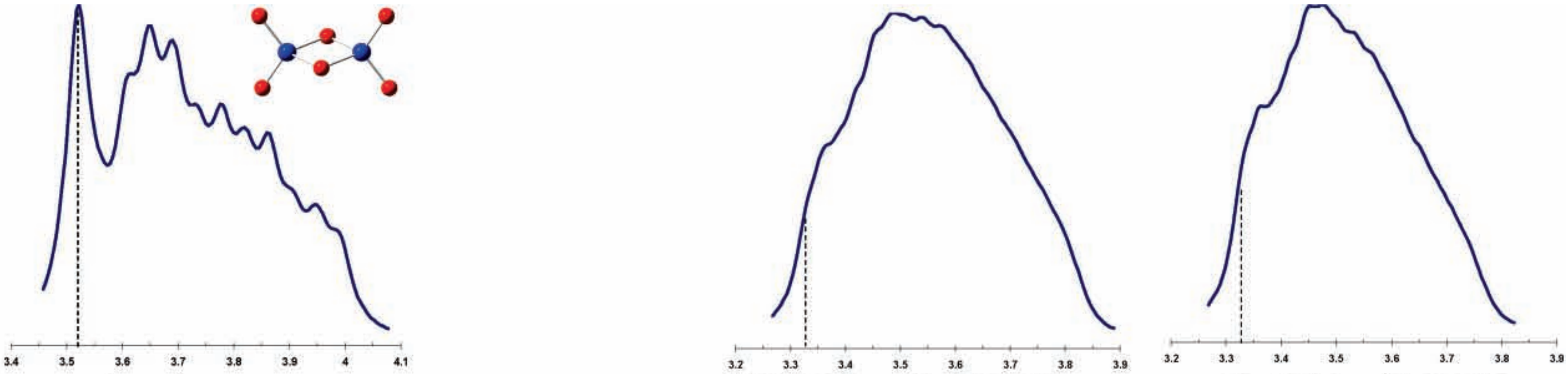

(a) $W_2O_6^-$, $^1A_g \leftarrow {}^2A_1$, B3LYP/aD

(d) $Mo_2O_6^-$, $^1A_g \leftarrow {}^2A_g$, B3LYP/aD

$Mo_2O_6^-$, $^1A_g \leftarrow {}^2A_g$ BP86/aD

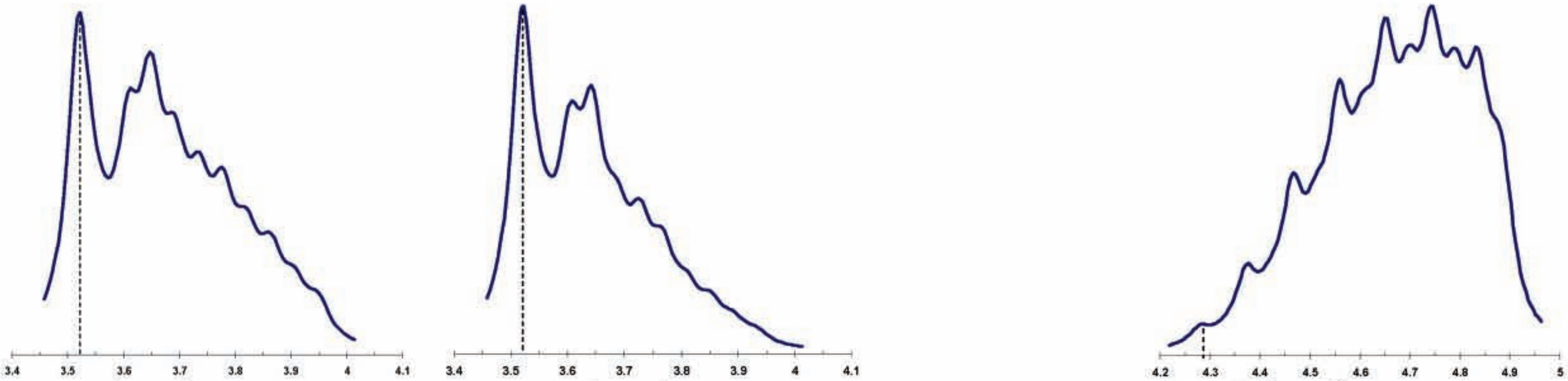

(b) $W_2O_6^-$, $^1A_g \leftarrow {}^2A_g$, B3LYP/aD

$W_2O_6^-$, $^1A_g \leftarrow {}^2A_g$ BP86/aD

(e) $Cr_2O_6^-$, $^1A_g \leftarrow {}^2A_1$, B3LYP/aD

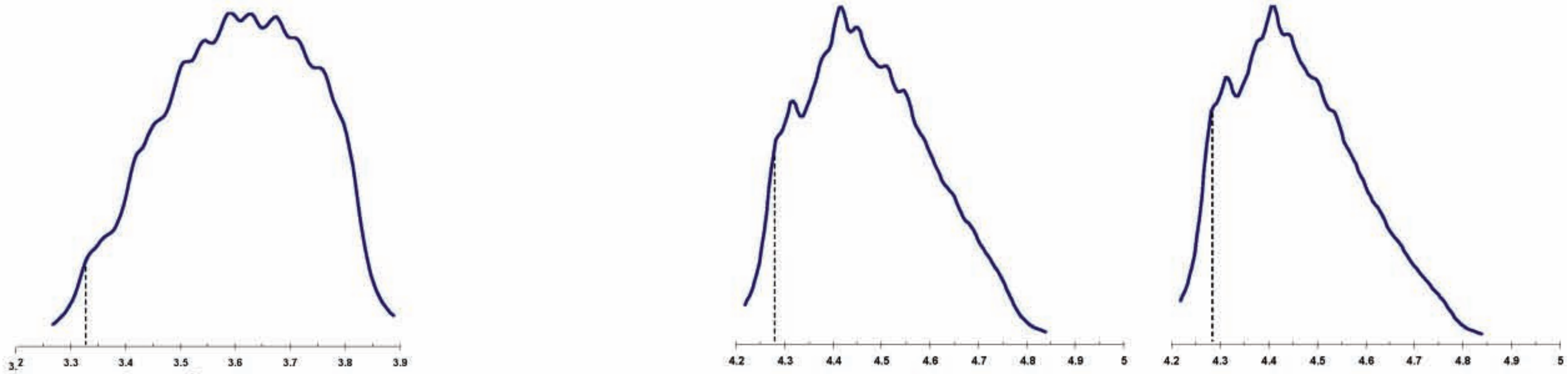

(c) $Mo_2O_6^-$, $^1A_g \leftarrow {}^2A_1$, B3LYP/aD

(f) $Cr_2O_6^-$, $^1A_g \leftarrow {}^2A_g$, B3LYP/aD

$Cr_2O_6^-$, $^1A_g \leftarrow {}^2A_g$, BP86/aD

Figure 2. Franck−Condon simulations of the photoelectron spectra of $M_2O_6^-$ at the B3LYP/aD and BP86/aD levels: (a) $W_2O_6^-$, $^1A_g \leftarrow {}^2A_1$; (b) $W_2O_6^-$, $^1A_g \leftarrow {}^2A_g$; (c) $Mo_2O_6^-$, $^1A_g \leftarrow {}^2A_1$; (d) $Mo_2O_6^-$, $^1A_g \leftarrow {}^2A_g$; (e) $Cr_2O_6^-$, $^1A_g \leftarrow {}^2A_1$; (f) $Cr_2O_6^-$, $^1A_g \leftarrow {}^2A_g$. The FWHM is 50 meV, and the vibrational temperature is 100 K.

TABLE 6: Adiabatic and Vertical Electron Detachment Energies (ADEs/VDEs, eV) for the Ground State of $M_2O_6^-$ (M = Cr, Mo, W) Calculated at the CCSD(T) Level with the B3LYP/aD Geometries and Compared with the Experimental Values

	ΔE_{aD}	ΔE_{aT}	ΔE_{aQ}	$\Delta E_{CBS}{}^a$	$\Delta E_{ZPE}{}^b$	$\Delta E_{CV}{}^c$	$\Delta E_{SR}{}^d$	$\Delta E_{total}{}^e$	expt
ADE									
$^1A_g \leftarrow {}^2A_1$									
$Cr_2O_6^-$	4.229	4.269	4.289	4.301	+0.028	−0.011 (+0.007)	+0.002	4.29	4.28(2)[f]
$Mo_2O_6^-$	3.246	3.196	3.207	3.214	+0.042	+0.081 (+0.086)	−0.004	3.33	
$W_2O_6^-$	3.278	3.234	3.252	3.262	+0.056	+0.104 (+0.112)	−0.003	3.42	3.52(2)[g]
$^1A_g \leftarrow {}^2A_g$									
$Cr_2O_6^-$	4.207	4.263	4.286	4.300	+0.035	+0.038 (+0.030)	−0.001	4.37	4.28(2)[f]
$Mo_2O_6^-$	3.245	3.204	3.215	3.223	+0.038	+0.089 (+0.096)	−0.004	3.35	
$W_2O_6^-$	3.305	3.264	3.283	3.294	+0.035	+0.100 (+0.109)	−0.003	3.43	3.52(2)[g]
VDE									
$^1A_g \leftarrow {}^2A_1$									
$Cr_2O_6^-$	4.538	4.614	4.660	4.687		+0.074 (+0.019)	+0.001	4.76	4.45(5)[f]
$Mo_2O_6^-$	3.472	3.527	3.569	3.593		+0.103 (+0.065)	−0.005	3.69	
$W_2O_6^-$	3.315	3.361	3.396	3.417		+0.141 (+0.105)	−0.003	3.56	3.63(2)[g]
$^1A_g \leftarrow {}^2A_g$									
$Cr_2O_6^-$	4.369	4.433	4.480	4.508		+0.067 (+0.031)	−0.003	4.57	4.45(5)[f]
$Mo_2O_6^-$	3.458	3.434	3.476	3.502		+0.105 (+0.068)	−0.005	3.60	
$W_2O_6^-$	3.427	3.395	3.430	3.452		+0.135 (+0.101)	−0.003	3.58	3.63(2)[g]

[a] Extrapolated using the mixed Gaussian/exponential formulas (ref 46) for the CCSD(T) energies with the aD, aT, and aQ basis sets. [b] B3LYP/aD for the $^1A_g \leftarrow {}^2A_1$ transition and BP86/aD for the $^1A_g \leftarrow {}^2A_g$ transition. [c] CCSD(T)/aug-cc-pwCVTZ/aug-cc-pwCVTZ-PP. The CCSD(T)/aug-cc-pwCVDZ/aug-cc-pwCVDZ-PP results are shown in the parentheses. [d] CISD/aT. [e] $\Delta E_{total} = \Delta E_{CBS} + \Delta E_{ZPE} + \Delta E_{CV} + \Delta E_{SR}$. [f] Reference 14. [g] Reference 15.

frequencies were calculated to be 285, 775, and 1109 cm^{-1} by B3LYP/aD, and 273, 746, and 1052 cm^{-1} by BP86/aD. These simulations are in good agreement with the experimental spectrum.

For $Mo_2O_6^-$, no experimental spectrum has been reported so far. Similar to the case of $Cr_2O_6^-$, the simulation for the $^1A_g \leftarrow {}^2A_1$ transition in Figure 2c is considerably broader than those for the $^1A_g \leftarrow {}^2A_g$ transition in Figure 2d.

Table 6 lists the calculated ADEs and VDEs with the CCSD(T) method and compared to the experimental results.[14,15] Experimental values for M = Mo are not yet available. We list results for both the $^2A_1$ and ^2A_g states. Geometries optimized at the B3LYP/aD level were used for the $^1A_g \leftarrow {}^2A_1$ transition, whereas they were optimized at the CCSD(T)/aD and CCSD(T)/aT levels for the $^1A_g \leftarrow {}^2A_g$ transition. The results for these two transitions are close to each other in most cases, so we focus on the $^1A_g \leftarrow {}^2A_1$ transition. For M = Cr, the calculated VDE at the CCSD(T)/CBS level is 0.32 eV larger than the experimental value, whereas for M = W, it is 0.07 eV smaller. The T_1 diagnostic ranges from 0.035 to 0.050 for M = Cr to from 0.025 to 0.040 for M = Mo and W. The good performance of the CCSD(T) method for M = W is likely due to there being less multireference character as found for the monomers. The VDE of $Mo_2O_6^-$ is likely to be very close to the calculated value of 3.69 eV, based on the above arguments. The basis set contributions to the calculated VDEs range from 0.10 to 0.15 eV, increasing the VDE with the size of the correction decreasing from Cr to Mo to W. The core−valence contributions range from 0.07 to 0.14 eV again increasing the VDE and the size of the contribution increases from Cr to Mo to W. The scalar relativistic effect is negligible. These observations are consistent with those for the monomers. Compared to the monomers, the basis set contribution for the dimers is slightly larger for M = Cr, but substantially larger for M = Mo and W, whereas the core−valence contribution is comparable for M = Cr and Mo, but slightly larger for M = W. The core−valence correction calculated with a smaller basis set at the CCSD(T)/aug-cc-pwCVDZ/aug-cc-pwCVDZ-PP level is about 0.04 eV smaller. In terms of the ADEs, the CCSD(T)/CBS value is about the same as the experimental value for M = Cr, and about 0.1 eV smaller for M = W. The basis set contribution to the ADE for M = Cr is half of that to the VDE, whereas for M = Mo and W it slightly reduces the ADE. The core−valence correction to the ADE is slightly negative for M = Cr, whereas it is substantially smaller than its contribution to the VDE for M = Mo and W. The scalar relativistic effect is again negligible. For the $^1A_g \leftarrow {}^2A_g$ transition, similar conclusions can be reached. Comparing the two states of the anions, the calculated ADEs and VDEs are essentially the same for M = W, both of which are slightly lower than the experimental values. For M = Mo, the calculated ADEs are nearly the same, whereas the VDEs differ by 0.1 eV. For M = Cr, the ADE of the ^2A_g state is larger than that of the $^2A_1$ state by 0.1 eV, whereas its VDE is smaller than the latter by 0.2 eV. This is consistent with the greater geometry difference for the $^2A_1$ state from ^1A_g states than for ^2A_g state.

Table 7 compares the calculated ADEs and VDEs from different DFT methods at the B3LYP/aD geometries for the $^2A_1$ state of the dimers to the experimental values. The CCSD(T)/CBS value will be used as the experimental value for M = Mo. In terms of the VDEs, the B3LYP method overestimates it by about 0.7 eV for M = Cr, whereas for M = Mo and W the B3LYP values are within 0.1 eV of the experimental values. Previous calculations[93] on the electron affinity of Cr_2O_6 with the B3LYP functional were done with the modest 6-31G* basis set (without diffuse functions). The calculated ADE of 4.27 eV and the calculated VDE of 4.71 eV are in better agreement with experiment than our B3LYP calculations with a better basis set with diffuse functions. This agreement with experiment occurs because with the anion is artificially destabilized without diffuse functions in the basis set. This comparison points out the need to use basis sets with adequate functions to describe the electronic structure. The performance of the DFT functionals for the dimer detachment energies is similar to the case of the monomers. For M = Cr, most hybrid functionals overestimate the VDE by more than 0.4 eV, except for the O3LYP and TPSSh methods, which overestimate it by 0.2−0.3 eV. In contrast, most pure functionals

TABLE 7: Adiabatic and Vertical Electron Detachment Energies (ADEs/VDEs, eV) for the Ground State of $M_2O_6^-$ (M = Cr, Mo, W) Calculated with Various Exchange−Correlation Functionals and aT Basis Sets at the B3LYP/aD Geometries and Compared to the CCSD(T) and Experimental Values[a]

	ADE			VDE		
method	$Cr_2O_6^-$	$Mo_2O_6^{-a}$	$W_2O_6^-$	$Cr_2O_6^-$	$Mo_2O_6^{-\ b}$	$W_2O_6^-$
B3LYP[c]	4.69 (+0.41)	3.49 (+0.16)	3.54 (+0.02)	5.13 (+0.68)	3.80 (+0.11)	3.68 (+0.05)
B3P86	5.12 (+0.84)	3.96 (+0.63)	4.06 (+0.54)	5.65 (+1.20)	4.40 (+0.71)	4.28 (+0.65)
B3PW91	4.56 (+0.28)	3.38 (+0.05)	3.47 (−0.05)	5.07 (+0.62)	3.81 (+0.12)	3.68 (+0.05)
B1B95	4.52 (+0.24)	3.25 (−0.08)	3.29 (−0.23)	5.09 (+0.64)	3.71 (+0.02)	3.54 (−0.09)
B1LYP	4.69 (+0.41)	3.36 (+0.03)	3.40 (−0.12)	5.16 (+0.71)	3.76 (+0.07)	3.57 (−0.06)
mPW1PW91	4.67 (+0.39)	3.39 (+0.06)	3.45 (−0.07)	5.24 (+0.79)	3.87 (+0.18)	3.70 (+0.07)
B98	4.65 (+0.37)	3.34 (+0.01)	3.40 (−0.12)	5.15 (+0.70)	3.75 (+0.06)	3.57 (−0.06)
B971	4.57 (+0.29)	3.27 (−0.06)	3.33 (−0.19)	5.04 (+0.59)	3.68 (−0.01)	3.51 (−0.12)
B972	4.39 (+0.11)	3.18 (−0.15)	3.27 (−0.25)	4.91 (+0.46)	3.63 (−0.06)	3.51 (−0.12)
PBE1PBE	4.61 (+0.33)	3.34 (+0.01)	3.41 (−0.11)	5.18 (+0.73)	3.83 (+0.14)	3.66 (+0.03)
O3LYP	4.15 (−0.13)	3.09 (−0.24)	3.22 (−0.30)	4.59 (+0.14)	3.54 (−0.15)	3.41 (−0.22)
TPSSh	4.36 (+0.08)	3.27 (−0.06)	3.38 (−0.14)	4.75 (+0.30)	3.59 (−0.10)	3.53 (−0.10)
BMK	5.87 (+1.59)	3.66 (+0.33)	3.38 (−0.14)	6.48 (+2.03)	4.18 (+0.49)	3.62 (−0.01)
SVWN5	4.09 (−0.19)	3.32 (−0.01)	3.56 (+0.04)	4.55 (+0.10)	3.73 (+0.04)	3.74 (+0.11)
BLYP	4.11 (−0.17)	3.21 (−0.12)	3.39 (−0.13)	4.30 (−0.15)	3.36 (−0.33)	3.35 (−0.28)
BP86	4.22 (−0.06)	3.38 (+0.05)	3.57 (+0.05)	4.49 (+0.04)	3.63 (−0.06)	3.60 (−0.03)
BPW91	4.09 (−0.19)	3.21 (−0.12)	3.41 (−0.11)	4.35 (−0.10)	3.47 (−0.22)	3.45 (−0.18)
BB95	3.95 (−0.33)	3.12 (−0.21)	3.30 (−0.22)	4.17 (−0.28)	3.33 (−0.36)	3.32 (−0.31)
PW91	4.17 (−0.11)	3.30 (−0.03)	3.49 (−0.03)	4.44 (−0.01)	3.55 (−0.14)	3.54 (−0.09)
mPWPW91	4.14 (−0.14)	3.27 (−0.06)	3.46 (−0.06)	4.40 (−0.05)	3.51 (−0.18)	3.50 (−0.13)
PBE	4.06 (−0.22)	3.23 (−0.10)	3.42 (−0.10)	4.33 (−0.12)	3.49 (−0.20)	3.46 (−0.17)
OLYP	3.84 (−0.44)	2.93 (−0.40)	3.10 (−0.42)	4.15 (−0.30)	3.25 (−0.44)	3.20 (−0.43)
TPSS	4.15 (−0.13)	3.24 (−0.09)	3.39 (−0.13)	4.43 (−0.02)	3.46 (−0.23)	3.40 (−0.23)
VSXC	4.15 (−0.13)	3.25 (−0.08)	3.37 (−0.15)	4.45 (+0.00)	3.50 (−0.19)	3.45 (−0.18)
HCTH93	3.95 (−0.33)	3.04 (−0.29)	3.23 (−0.29)	4.28 (−0.17)	3.38 (−0.31)	3.37 (−0.26)
HCTH147	4.13 (−0.15)	3.31 (−0.02)	3.44 (−0.08)	4.46 (+0.01)	3.58 (−0.11)	3.55 (−0.08)
HCTH407	4.10 (−0.18)	3.24 (−0.09)	3.41 (−0.11)	4.44 (−0.01)	3.59 (−0.10)	3.56 (−0.07)
CCSD(T)	4.29 (+0.01)	3.33	3.42 (−0.10)	4.76 (+0.31)	3.69	3.56 (−0.07)
expt	4.28 ± 0.02		3.52 ± 0.02	4.45 ± 0.05		3.63 ± 0.02

[a] The difference between the calculated and experimental values is shown in the parentheses. [b] The CCSD(T) value is used as the experimental value. [c] At the B3LYP/aD level, the ADEs are calculated to be 4.69, 3.55, and 3.61 eV, and the VDEs are calculated to be 5.13, 3.86, and 3.70 eV for M = Cr, Mo, and W, respectively.

yield VDEs within 0.1 eV of the experimental value with the largest deviations (−0.3 eV) given by the BB95 and OLYP methods. For M = Mo and W, the VDEs calculated by using most hybrid functionals agree with the experimental values within 0.1 eV. The B3P86 functional overestimates the VDE by ~0.7 eV for M = Mo and W, whereas the BMK functional overestimates it by 0.5 eV for M = Mo. Most pure functionals underestimate the VDEs by more than 0.2 eV for M = Mo and W. The calculated ADEs follow similar trends.

To compare the overall performance of the exchange−correlation functionals in the calculations of the VDEs of these oxides, we consider the case for M = Cr separately from M = Mo and W. For CrO_3^- and $Cr_2O_6^-$, O3LYP is the only hybrid functional to give a maximum error less than 0.15 eV. Among the pure functionals, the SVWN5, BP86, PW91, mPWPW91, TPSS, VSXC, and HCTH407 functionals give a maximum error within 0.15 eV. For MoO_3^-, WO_3^-, and $W_2O_6^-$, the B1B95, B98, and BP86 functionals give a maximum error within 0.1 eV. For the VDEs of all these molecules, the BP86 functional consistently yields a maximum error of 0.06 eV with an average error of 0.03 eV. The PW91 and SVWN5 functionals have an average error of less than 0.1 eV, but not as good as the BP86 functional. Surprisingly, the SVWN5 local density approximation functional is quite good for the calculations of the VDEs of these oxides.

Heats of Formation. Table 8 lists the extrapolated CCSD(T)/CBS valence electronic energies with different extrapolation schemes and Table 9 lists the atomization energies at 0 K calculated at the CCSD(T) level. The atomization energies were also calculated at the B3LYP, BP86, and PW91 levels, and these can be found in the Supporting Information. At the CCSD(T) level, the CBS energy can be obtained with the three-parameter, mixed Gaussian/exponential formula[46] using the aD, aT, and aQ energies.

TABLE 8: CCSD(T)/CBS Contribution to the Atomization Energies in kcal/mol (ΔE_{CBS}) Calculated with Different Extrapolation Schemes

molecule	ΔE_{CBS} eq 5[a]	ΔE_{CBS} eq 5[b]	ΔE_{CBS} eq 5[c]	ΔE_{CBS} eq 6[d]	ΔE_{CBS} eq 6[e]	ΔE_{CBS} eq 6[f]	ΔE_{CBS}[g] av
CrO_3	342.16	341.72	342.04	347.12	342.93	344.84	341.97
Cr_2O_6	777.61	776.65	777.36				777.21
MoO_3	417.91	417.33	417.77	423.18	418.83	420.83	417.67
Mo_2O_6	948.04	946.83	947.74				947.54
WO_3	476.37	475.74	476.19	481.99	477.59	479.68	476.10
W_2O_6	1081.63	1080.33	1081.27				1081.08

[a] Extrapolated values using the mixed Gaussian/exponential formula eq 5 for the CCSD(T)/aD, CCSD(T)/aT, and CCSD(T)/aQ energies. Cardinal numbers of 2, 3, and 4 for the aD, aT, and aQ basis sets were used for O, and 3, 4, and 5 for M and M_nO_{3n} (M = Cr, Mo, W). [b] Extrapolated values using the mixed Gaussian/exponential formula eq 5 for the CCSD(T)/aD, CCSD(T)/aT, and CCSD(T)/aQ energies. Cardinal numbers of 2, 3, and 4 for the aD, aT, and aQ basis sets were used. [c] Extrapolated values using the mixed Gaussian/exponential formula eq 5 for the CCSD(T)/aD, CCSD(T)/aT, and CCSD(T)/aQ energies. Cardinal numbers of 2, 3, and 4 for the aD, aT, and aQ basis sets were used for O, 3, 4, and 5 for M, and 2.5, 3.5, and 4.5 for M_nO_{3n}. [d] Extrapolated values using the two-parameter inverse cubic formula eq 6 for the CCSD(T)/aQ and CCSD(T)/a5 energies. Cardinal numbers of 4 and 5 were used for O, and 5 and 6 for M and MO_3. [e] Extrapolated values using the two-parameter inverse cubic formula eq 6 for the CCSD(T)/aQ and CCSD(T)/a5 energies. Cardinal numbers of 4 and 5 for the aQ and a5 basis sets were used. Extrapolation of the Hartree−Fock (HF) and correlation energy components separately gives values of 342.82, 418.55, and 477.43 kcal/mol for MO_3 (M = Cr, Mo, W), which are smaller than those from the sixth column by <0.5 kcal/mol. [f] Extrapolated using the two-parameter inverse cubic formula eq 6 for the CCSD(T)/aQ and CCSD(T)/a5 energies. Cardinal numbers of 4 and 5 were used for O, 5 and 6 for M, and 4.5 and 5.5 for MO_3. Extrapolation of the HF and correlation energy components separately gives values of 344.35, 420.12, and 479.12 kcal/mol for MO_3 (M = Cr, Mo, W), which are smaller than those from the seventh column by <1 kcal/mol. [g] The average of columns 2, 3, and 4.

TABLE 9: Atomization Energies in kcal/mol at 0 K ($\Sigma D_{0,0K}$) Calculated at the CCSD(T) Level

molecule	ΔE_{CBS}[a] av	ΔE_{ZPE}[b]	ΔE_{CV}[c]	ΔE_{MVD}[d]	ΔE_{DK}[e]	ΔE_{SO}[f]	$\Sigma D_{0,0K}$[g] (MVD)	$\Sigma D_{0,0K}$[h] (DK)
CrO_3	341.97	−5.61	2.90	−2.09	−4.97	−0.67	336.5	333.6
Cr_2O_6	777.21	−13.66	9.44	−5.03	−10.78	−1.34	766.6	760.9
MoO_3	417.67	−5.35	0.17	−0.63	0.94	−0.67	411.2	412.8
Mo_2O_6	947.54	−12.36	3.82	−1.57	1.14	−1.34	936.1	938.8
WO_3	476.10	−5.38	−0.94	−0.61		−0.67	460.1[i]	
W_2O_6	1081.08	−12.12	−0.44	−1.51		−1.34	1048.8[i]	

[a] Average values for the CBS valence electronic energy from Table 8. See text for details. [b] CCSD(T)/aT for the monomers and B3LYP/aD for the dimers. [c] CCSD(T)/aug-cc-pwCVTZ/aug-cc-pwCVTZ-PP. When calculated without the extra diffuse functions, ΔE_{CV} becomes +2.47 and −0.79 kcal/mol for MO_3 (M = Cr, Mo), and 8.08 and 1.25 kcal/mol for M_2O_6. [d] Expectation values of the MVD terms at the CISD/aT level. [e] The difference between the atomization energies calculated at the CCSD(T)/cc-pwCVTZ/cc-pwCVTZ-PP and CCSD(T)-DK/cc-pwCVTZ-DK levels. All electrons were correlated except for those in the Cr 1s2s2p and Mo 1s2s2p3s3p3d orbitals for the CCSD(T)-DK calculations. [f] The spin−orbit splitting is −0.223 kcal/mol for the ground state ($^3P_2$) of O, 0.0 kcal/mol for the ground state ($^7S_3$) of Cr or Mo and the first excited state ($^7S_3$) of W. [g] $\Sigma D_{0,0K} = \Delta E_{CBS} + \Delta E_{ZPE} + \Delta E_{CV} + \Delta E_{MVD} + \Delta E_{SO}$, where $\Delta E = nE(M,{}^7S_3) + 3nE(O,{}^3P_2) - E(M_nO_{3n})$. [h] $\Sigma D_{0,0K} = \Delta E_{CBS} + \Delta E_{ZPE} + \Delta E_{CV} + \Delta E_{DK} + \Delta E_{SO}$. [i] The calculated atomization energy was corrected by the experimental energy difference between the first excited state ($^7S_3$) and the ground state ($^5D_0$) of W (8.43 kcal/mol).

$$E(n) = E_{CBS} + Be^{-(n-1)} + Ce^{-(n-1)2} \qquad (5)$$

The cardinal numbers for the aD, aT, and aQ basis sets can be different because of the differences in the highest angular momentum value of the basis set (l_{max}) on the O and the metal. Thus we calculated three sets of extrapolated values: (1) use 2, 3, and 4 as the cardinal numbers for O, and 3, 4, and 5 for M, MO_3, and M_2O_6; (2) use 2, 3, and 4 as the cardinal numbers for the aD, aT, and aQ basis sets for all atoms and molecules; and (3) use 2, 3, and 4 as the cardinal numbers for O, 3, 4, and 5 for M, and 2.5, 3.5, and 4.5 for MO_3 and M_2O_6 with the latter recommendation coming from the work of Peterson.[42] The ΔE_{CBS} values determined with these different values for n vary by 0.3−1.3 kcal/mol. The largest values for ΔE_{CBS} were found with the first set and the smallest with the second set. For the monomers, we also calculated the CCSD(T) energies with the aug-cc-pV5Z and aug-cc-pV5Z-PP basis sets (a5). We can also calculate the CBS value using the two-parameter, inverse cubic formula[94] with the aQ and a5 energies.

$$E(l_{max}) = E_{CBS} + B/l_{max}{}^3 \qquad (6)$$

We used the same cardinal number sets for this extrapolation as for the extrapolations with eq 5. The ΔE_{CBS} values are larger than the values from eq 5 and show a much larger variation of up to 4.4 kcal/mol; they display the same trends as those for eq 5 in terms of the different sets. We also extrapolated the Hartree−Fock (HF) and correlation energy components separately for the monomers. The HF energy was extrapolated using an exponential formula[95] with the aT, aQ, and a5 energies,

$$E(n) = E_{CBS} + Be^{-C*n} \qquad (7)$$

whereas the correlation energy was extrapolated using eq 6 with the aQ and a5 energies. The results from this extrapolation scheme are 0.5−1 kcal/mol smaller than those from a single extrapolation of the total valence electronic energy using eq 6. Because of the much larger sensitivity of the extrapolated values for eq 6 in terms of which cardinal numbers are employed, we have not used these in the heats of formation predictions. We have averaged the different extrapolated values from eq 5 and used this average in the prediction of the heats of formation in Table 9.

The core−valence energy was calculated at the CCSD(T)/aug-cc-pwCVTZ/aug-cc-pwCVTZ-PP level, and for M = Cr and Mo also at the CCSD(T)/cc-pwCVTZ/cc-pwCVTZ-PP level. The core−valence correction calculated with the augmented sets is larger by 0.5−2.5 kcal/mol than those obtained without the augmented diffuse functions.

We calculated the relativistic correction as the expectation values for the two dominant terms in the Breit−Pauli Hamiltonian, the so-called mass-velocity and one-electron Darwin (MVD) corrections from CISD/aT calculations. For M = Cr and Mo, we also calculated the relativistic correction as the difference between the atomization energies at the CCSD(T)/cc-pwCVTZ/cc-pwCVTZ-PP and CCSD(T)-DK/cc-pwCVTZ-DK levels.[96] To be consistent, the Cr 1s2s2p orbitals and the Mo 1s2s2p3s3p3d orbitals were excluded from the correlation treatment in the DK calculations. This will also enable us to account for any additional issues with the effects of the ECP. For M = Cr, the relativistic correction calculated by the latter approach is about two times more negative than the MVD correction. For M = Mo, the results from both approaches are small, but their signs are different. The contributions to the total atomization energies from the core−valence and scalar relativistic effects are larger for M = Cr than M = Mo and W.

The atomization energy increases as one goes down the triad from M = Cr to Mo to W, and that of the dimer is more than twice of the monomer. This is consistent with the substantial stabilization energy for forming the dimer from two monomers.[16]

To calculate the heats of formation, we used the total atomization energies calculated with the DK correction for the Cr and Mo oxides and with the MVD correction for the W oxides. Table 10 gives the calculated heats of formation at 0 and 298 K and compares with the experimental values at 0 K. An issue with calculating reliable heats of formation is that there is much more uncertainty in the heats of formation of the metal atoms then we usually find in main group elements. The uncertainties are ±1.0, ±0.9, and ±1.5 kcal/mol for Cr, Mo, and W, respectively. For example, the use of these values introduces an error of 3 kcal/mol for $\Delta H_f(W_2O_6)$ irrespective of the errors in the electronic structure calculations. There is also an error of up to ±2.0 kcal/mol in the electronic structure calculations due to errors in the ECP and in the extrapolation procedure. We note that the experimental heats of formation for the clusters have substantial uncertainties of up to ±10 kcal/mol. The CCSD(T)/CBS heats of formation are in good agreement with the experimental data, and they are within the uncertainties of the experimental values except for WO_3. We suggest that this value needs to be remeasured. The calculated heat of formation for W_2O_6 is within the experimental error limits when the error limits in the calculations are included.

The B3LYP functional significantly underestimates the CCSD(T) heats of formation for CrO_3 by 21 kcal/mol. The use

TABLE 10: Heats of Formation in kcal/mol at 0 and 298 K ($\Delta H_{f,0K}$ and $\Delta H_{f,298K}$) Calculated with the CCSD(T), B3LYP, BP86, and PW91 Methods,[a] and Compared with the Experimental Values

	CCSD(T)[b]		B3LYP[c]		BP86[c]		PW91[c]		expt[d]
molecule	$\Delta H_{f,0K}$[e]	$\Delta H_{f,298K}$[f]	$\Delta H_{f,0K}$[e]	$\Delta H_{f,298K}$[f]	$\Delta H_{f,0K}$[e]	$\Delta H_{f,298K}$[f]	$\Delta H_{f,0K}$[e]	$\Delta H_{f,298K}$[f]	$\Delta H_{f,0K}$
CrO_3	−62.2	−63.1	−41.3	−42.2	−112.8	−113.8	−111.9	−112.8	−69 ± 10
Cr_2O_6	−218.0	−219.9	−174.1	−176.7	−318.0	−320.5	−317.8	−320.4	
MoO_3	−78.7	−79.7	−71.5	−72.5	−123.1	−124.0	−122.8	−123.8	82 ± 5
Mo_2O_6	−270.7	−272.6	−251.0	−252.9	−350.8	−352.7	−352.0	−353.9	
WO_3	−80.0	−81.1	−70.6	−71.7	−110.7	−111.8	−110.8	−111.9	69 ± 7
W_2O_6	−288.7	−290.7	−262.1	−264.1	−335.9	−337.8	−338.0	−339.9	277 ± 10

[a] Error bars due to errors in the heats of formation of the atoms are ± 1.0 for CrO_3, ±2.0 for Cr_2O_6, ±0.9 for MoO_3, ±1.8 for Mo_2O_6, ±1.5 for WO_3, and ± 3.0 for W_2O_6. [b] Atomization energies shown in Table 9. For the CCSD(T) method, the DK correction was used for M = Cr and Mo, whereas the MVD correction was used for M = W. [c] Atomization energies calculated at the B3LYP/aT, BP86/aT, and PW91/aT levels with the B3LYP/aD geometries. See Supporting Information. [d] Reference 81. [e] $\Delta H_{f,0K}(M_nO_{3n}) = n\Delta H_{f,0K}(M) + 3n\Delta H_{f,0K}(O) - \Sigma D_{0,0K}(M_nO_{3n})$, where the experimental $\Delta H_{f,0K}$ (58.98 ± 0.02, 94.5 ± 1.0, 157.1 ± 0.9, 203.1 ± 1.5 kcal/mol for O, Cr, Mo, W) were used for the atoms. [f] $\Delta H_{f,298K}(M_nO_{3n}) = \Delta H_{f,0K}(M_nO_{3n}) + \Delta H_{0K\rightarrow 298K}(M_nO_{3n}) - n\Delta H_{0K\rightarrow 298K}(M) - 3n\Delta H_{0K\rightarrow 298K}(O)$. The experimental enthalpy change from 0 to 298 K ($\Delta H_{0K\rightarrow 298K}$) is 1.04, 0.97, 1.10, and 1.19 kcal/mol for O, Cr, Mo, and W, respectively.

TABLE 11: Dimerization Energies in kcal/mol at 0 and 298 K (ΔE_{0K} and ΔH_{298K}) Calculated at the CCSD(T), B3LYP, BP86, and PW91 Levels from the Heats of Formation in Table 10

	CCSD(T)		B3LYP		BP86		PW91		expt
	ΔE_{0K}	ΔH_{298K}	ΔE_{0K}	ΔH_{298K}	ΔE_{0K}	ΔH_{298K}	ΔE_{0K}	ΔH_{298K}	ΔE_{0K}
$CrO_3 \rightarrow Cr_2O_6$	−93.6	−93.9	−91.5	−92.3	−92.4	−92.9	−94.0	−94.8	
$MoO_3 \rightarrow Mo_2O_6$	−113.3	−113.2	−108.0	−107.9	−104.6	−104.7	−106.4	−106.3	
$WO_3 \rightarrow W_2O_6$	−128.7	−128.5	−120.9	−120.7	−114.5	−114.2	−116.4	−116.1	139 ± 24

of this functional to predict the heats of formation for MoO_3 and WO_3 gives results that are much closer to the CCSD(T) values, with a difference of 7 kcal/mol for MoO_3 and 9 kcal/mol for WO_3. The BP86 and PW91 functionals yield similar results for the heats of formation, and they substantially overestimate the CCSD(T) values. The agreement between B3LYP and CCSD(T) is much worse for the heats of formation of the dimers with differences of 44, 20, and 27 kcal/mol for M = Cr, Mo, and W, respectively; the differences follow the same trend as found for the monomers. The BP86 and PW91 functionals yield much worse results for the heats of formation of the dimers as expected. To provide more insight as to why the BP86 and PW91 methods give such poor results for the heats of formation of the metal oxides, we calculated the dissociation energy at 0 K for the ground state of O_2. The accurate experimental value is 118.0 kcal/mol.[97] The results from the BP86/aT//B3LYP/aD and PW91/aT//B3LYP/aD calculations are 139.1 and 140.3 kcal/mol, respectively, whereas those from the B3LYP/aT//B3LYP/aD and CCSD(T)/CBS calculations are 120.8 and 118.1 kcal/mol. Thus the BP86 and PW91 functionals seem to predict overbinding when O atoms are present.

The average M═O μ-oxo bond energies at 0 K for MO_3 can be calculated by dividing the total atomization energies ($\Sigma D_{0,0K}$) by the number of M═O bonds, which is 3 for MO_3, to yield 111.2, 137.6, and 153.4 kcal/mol for M = Cr, Mo, and W, respectively, at the CCSD(T)/CBS level. Thus these metal μ-oxo bond energies are quite large and increase as one goes down the group. The metal μ-oxo bonds are expected to be strong due to the interaction between the filled O pπ orbitals and the empty M dπ orbitals.[98] The Cr═O bond is much weaker than the Mo═O bond, which is again weaker than the W═O bond, even though the M═O bond length significantly increases from M = Cr to Mo and W, as shown in Table 2. The ionic character of MO_3 increases from M = Cr to Mo to W,[16] resulting in much stronger metal oxygen π bonding due to the much reduced electron population in the metal dπ orbitals for the heavier metals. Thus, the W═O bond is much stronger than the Mo═O bond, which is much stronger than the Cr═O bond.

If we assume that the M═O bond energies in MO_3 are the same as in M_2O_6, then we can estimate the strength of the M−O bridge bonds in M_2O_6 as follows: $E(\text{M}-\text{O}) = {}^1/_4[\Sigma D_{0,0K}(M_2O_6) - 4E(\text{M}═\text{O})]$. This gives E(M−O) as 78.0, 97.1, and 108.8 kcal/mol for M = Cr, Mo, and W, respectively, at the CCSD(T)/CBS level, which follows the same trend as that for the M═O bond energies. The above arguments about the bond energies of the M═O bonds also apply to those of the M−O bonds.

The dimerization energies of MO_3 to form M_2O_6 can be calculated from the CCSD(T) heats of formation in Table 9, and these are shown in Table 10. The values for the dimerization energy increase from M = Cr to M = W as we have shown previously.[16] The dimerization energies at 0 K are large, 93.6, 113.3, and 128.7 kcal/mol at the CCSD(T)/CBS level. The dimerization energy is consistent with two M═O μ-oxo bonds being broken and four M−O bridge bonds being formed. The CCSD(T) and DFT dimerization energies are approximately the same for M = Cr. The difference between the CCSD(T) and DFT dimerization energies increases for M = Mo and the pure DFT functionals give dimerization energies that are lower than the hybrid B3LYP functional as found previously.[16] The differences between the CCSD(T) and DFT values are 5−9 kcal/mol for M = Mo and even larger for M = W. The dimerization energy for WO_3 is in good agreement with the experimental value considering the large experimental error limits.

Conclusions

We have benchmarked the electron detachment energies of MO_3^- and $M_2O_6^-$ (M = Cr, Mo, W) at the DFT and CCSD(T) levels. Photoelectron spectra from the ground state of the anion to the neutral cluster have been simulated and are consistent with a reassignment of the previously reported VDE of 3.66(2) eV for CrO_3^- to 3.77(2) eV.[83] Our calculations show that the B3LYP bond lengths are shorter than their CCSD(T) counterparts by 0.01−0.02 Å for M = Cr, whereas they are essentially the same for M = Mo and W. The CCSD(T) method overestimates the detachment energies for M = Cr with a larger error for the VDE than for the ADE, likely due to the multireference character of the wavefunctions. For M = Mo and W, the CCSD(T) method reproduces the experimental values to better than 0.1 eV if sufficiently large basis sets and core−valence corrections are included. Nearly all of the hybrid functionals give poor detachment energies for M = Cr, whereas their performance is much better for M = Mo and W. This is consistent with the fact that CCSD(T) based on a Hartree−Fock wavefunction also does not perform particularly well for M = Cr but does much better for M = Mo and W. Many of the pure gradient-corrected functionals predict reasonable electron affinities for M = Cr but, except for BP86, SVWN5 and PW91, most of the pure functionals do not perform as well for M = Mo and W. Among all of the functionals we have benchmarked, the BP86 method yields the best results for the VDEs with a maximum error of 0.06 eV and an average error of 0.03 eV. The PW91 functional also predicts reasonable VDEs for these metal oxides. Both the BP86 and PW91 functionals can be used to predict reasonable ADEs for these species except for WO_3, where the error is 0.3−0.4 eV, although this deviation could be due to the fact that the ADE is not as well-determined experimentally as is the VDE in this case. Heats of formation calculated at the CCSD(T) level are in reasonable agreement with the experimental values considering the large error limits. At the DFT level, only the B3LYP functional gives qualitatively correct heats of formation for these metal oxides but with errors as large as 21 and 44 kcal/mol for CrO_3 and Cr_2O_6. The predicted heats of formation from the BP86 and PW91 methods are substantially larger than the CCSD(T) and experimental results. The results that we have obtained show that highly accurate measurements of the heats of formation of the gas-phase metal atoms and small molecules are needed to improve the computational benchmarking procedure.

Acknowledgment. We thank Prof. L.-S. Wang (Washington State University and PNNL) for helpful discussions and Prof. K. Peterson (Washington State University) for providing the transition metal basis sets before publication as well as for many discussions on the topic of extrapolating energies for transition metal systems to the complete basis set limit. This work was supported by the Chemical Sciences, Geosciences and Biosciences Division, Office of Basic Energy Sciences, U.S. Department of Energy (DOE) under grant no. DE-FG02-03ER15481 (catalysis center program). D.A.D. also thanks the Robert Ramsay Chair Fund of The University of Alabama for support. Part of this work was performed at the W. R. Wiley Environmental Molecular Sciences Laboratory, a national scientific user facility sponsored by DOE's Office of Biological and Environmental Research and located at Pacific Northwest National Laboratory, operated for the DOE by Battelle.

Supporting Information Available: Zero-point energies and electronic energies (E_e) at different computational levels calculated at the B3LYP/aD, BP86/aD, CCSD(T)/aD, CCSD(T)/aT, and CCSD(T)/aT-ECP optimized geometries. The T_1 diagnostic in the CCSD(T) calculations are also listed. Cartesian coordinates in Angstroms optimized at the B3LYP/aD, BP86/aD, CCSD(T)/aD, CCSD(T)/aT, and CCSD(T)/aT-ECP levels. This material is available free of charge via the Internet at http://pubs.acs.org.

References and Notes

(1) (a) Pope, M. T., Müller, A., Eds. *Polyoxometalates: from Platonic Solids to Retro-viral Activity*; Kluwer Academic Publishers: Dodrecht, The Netherlands, 1994. (b) Hill, C. L., Ed. A special issue on polyoxometalates in catalysis. *J. Mol. Catal. A: Chem*. **1996**, *114*, 1−371. (c) Hill, C. L., Ed. A special issue on polyoxometalates. *Chem. Rev.* **1998,** *98,* 1−390.

(2) Parr, R. G.; Yang, W. *Density-Functional Theory of Atoms and Molecules*; Oxford University Press: New York, 1989.

(3) Sosa, C.; Andzelm, J.; Elkin, B. C.; Wimmer, E.; Dobbs, K. D.; Dixon, D. A. *J. Phys. Chem.* **1992**, *96*, 6630.

(4) Ziegler, T. *Chem. Rev.* **1991**, *91*, 651.

(5) Schultz, N. E.; Zhao, Y.; Truhlar, D. G. *J. Phys. Chem. A* **2005**, *109*, 4388.

(6) Zhao, Y.; Truhlar, D. G. *J. Chem. Phys.* **2006**, *124*, 224105.

(7) Furche, F.; Perdew, J. P. *J. Chem. Phys.* **2006**, *124*, 044103.

(8) Becke, A. D. *Phys. Rev. A* **1988**, *38*, 3098.

(9) Lee, C.; Yang, W.; Parr, R. G. *Phys. Rev. B* **1988**, *37*, 785.

(10) Perdew, J. P. *Phys. Rev. B* **1986**, *33*, 8822.

(11) Tao, J. M.; Perdew, J. P.; Staroverov, V. N.; Scuseria, G. E. *Phys. Rev. Lett.* **2003**, *91*, 146401.

(12) Gutsev, G. L.; Jena, P.; Zhai, H.-J.; Wang, L.-S. *J. Chem. Phys.* **2001**, *115*, 7935.

(13) Zhai, H.-J.; Kiran, B.; Cui, L.-F.; Li, X.; Dixon, D. A.; Wang, L.-S. *J. Am. Chem. Soc.* **2004**, *126*, 16134.

(14) Zhai, H.-J.; Huang, X.; Cui, L.-F.; Li, X.; Li, J.; Wang, L.-S. *J. Phys. Chem. A* **2005**, *109*, 6019.

(15) Zhai, H.-J.; Wang, L.-S. *J. Chem. Phys.* **2006**, *125*, 164315.

(16) Li, S.; Dixon, D. A. *J. Phys. Chem. A* **2006**, *110*, 6231.

(17) Becke, A. D. *J. Chem. Phys.* **1993**, *98*, 5648.

(18) Slater, J. C. *Quantum Theory of Molecules and Solids*; McGraw-Hill: New York 1974; Vol. 4.

(19) Vosko, S. H.; Wilk, L.; Nusair, M. *Can. J. Phys.* **1980**, *58*, 1200.

(20) Perdew, J. P.; Wang, Y. *Phys. Rev. B* **1991**, *45*, 13244.

(21) Becke, A. D. *J. Chem. Phys.* **1996**, *104*, 1040.

(22) Burke, K.; Perdew, J. P. Wang. Y. In *Electronic Density Functional Thoery: Recent Progress and New Directions*; Dobson, J. F., Vignale, G., Das, M. P., Eds.; Plenum: New York 1998.

(23) Adamo, C.; Barone, V. *J. Chem. Phys.* **1998**, *108*, 664.

(24) Perdew, J. P.; Burke, K.; Ernzerhof, M. *Phys. Rev. Lett.* **1996**, *77*, 3865.

(25) Perdew, J. P.; Burke, K.; Ernzerhof, M. *Phys. Rev. Lett.* **1997**, *78*, 1396.

(26) Handy, N. C.; Cohen, A. J. *Mol. Phys.* **2001**, *99*, 403.

(27) Cohen, A. J.; Handy, N. C. *Mol. Phys.* **2001**, *99*, 607.

(28) Bohmann, J. A.; Weinhold, F.; Farrar, T. C. *J. Chem. Phys.* **1997**, *107*, 1173.

(29) Ruud, K.; Helgaker, T.; Bour, P. *J. Phys. Chem. A* **2002**, *106*, 7448.

(30) Helgaker, T.; Ruud, K.; Bak, K. L.; Jorgensen, P.; Olsen, J. *Faraday Discuss.* **1994**, *99*, 165.

(31) Adamo, C.; Barone, V. *Chem. Phys. Lett.* **1997**, *274*, 242.

(32) Schmider, H. L.; Becke, A. D. *J. Chem. Phys.* **1998**, *108*, 9624.

(33) Hamprecht, F. A.; Cohen, A. J.; Tozer, D. J.; Handy, N. C. *J. Chem. Phys.* **1998**, *109*, 6264.

(34) Wilson, P. J.; Bradley, T. J.; Tozer, D. J. *J. Chem. Phys.* **2001**, *115*, 9233.

(35) Van, Voorhis, T.; Scuseria, G. E. *J. Chem. Phys.* **1998**, *109*, 400.

(36) Boese, A. D.; Martin, J. M. L. *J. Chem. Phys.* **2004**, *121*, 3405.

(37) Purvis, G. D., III; Bartlett, R. J. *J. Chem. Phys.* **1982**, *76*, 1910.

(38) Raghavachari, K.; Trucks, G. W.; Pople, J. A.; Head-Gordon, M. *Chem. Phys. Lett.* **1989**, *157*, 479.

(39) Watts, J. D.; Gauss, J.; Bartlett, R. J. *J. Chem. Phys.* **1993**, *98*, 8718.

(40) Bartlett, R.J.; Musial, M. *Rev. Mod. Phys.* **200**7, *79*, 291.

(41) Kendall, R. A.; Dunning, T. H., Jr.; Harrison, R. J. *J. Chem. Phys.* **1994**, *96*, 6796.

(42) Peterson, K.A.; Figgen, D.; Dolg, M.; Stoll, H. *J. Chem. Phys.* **2007**, *126*, 124101. Peterson, K.A. Unpublished basis sets for Cr and W.

(43) Dolg, M.; Stoll, W. H.; Preuss, H. *J. Chem. Phys.* **1987**, *86*, 866.

(44) Andrae, D.; Haeussermann, U.; Dolg, M.; Stoll, H.; Preuss, H. *Theor. Chim. Acta* **1990**, *77*, 123.

(45) Martin, J. M. L.; Sundermann, A. *J. Chem. Phys.* **2001**, *114*, 3408.

(46) Peterson, K. A.; Woon, D. E.; Dunning, T. H., Jr. *J. Chem. Phys.* **1994**, *100*, 7410.

(47) Woon, D. E.; Dunning, T. H., Jr. *J. Chem. Phys.* **1995**, *103*, 4572.

(48) Peterson, K. A.; Dunning, T. H., Jr. *J. Chem. Phys.* **2002**, *117*, 10548.

(49) Peterson, K. A.; Xantheas, S. S.; Dixon, D. A.; Dunning, T. H., Jr. *J. Phys. Chem. A* **1998**, *102*, 2449.

(50) Feller, D.; Peterson, K. A. *J. Chem. Phys.* **1998**, *108*, 154.

(51) Dixon, D. A.; Feller, D. *J. Phys. Chem. A* **1998**, *102*, 8209.

(52) Feller, D.; Peterson, K. A. *J. Chem. Phys.* **1999**, *110*, 8384.

(53) Feller, D.; Dixon, D. A. *J. Phys. Chem. A* **1999**, *103*, 6413.

(54) Feller, D. *J. Chem. Phys.* **1999**, *111*, 4373.

(55) Feller, D.; Dixon, D. A. *J. Phys. Chem. A* **2000**, *104*, 3048.

(56) Feller, D.; Sordo, J. A. *J. Chem. Phys.* **2000**, *113*, 485.

(57) Feller, D.; Dixon, D. A. *J. Chem. Phys.* **2001**, *115*, 3484.

(58) Dixon, D. A.; Feller, D.; Sandrone, G. *J. Phys. Chem. A* **1999**, *103*, 4744.

(59) Ruscic, B.; Wagner, A. F.; Harding, L. B.; Asher, R. L.; Feller, D.; Dixon, D. A.; Peterson, K. A.; Song, Y.; Qian, X.; Ng, C.; Liu, J.; Chen, W.; Schwenke, D. W. *J. Phys. Chem. A* **2002**, *106*, 2727.

(60) Feller, D.; Dixon, D. A.; Peterson, K. A. *J. Phys. Chem. A* **1998**, *102*, 7053.

(61) Dixon, D. A.; Feller, D.; Peterson, K. A. *J. Chem. Phys*. **2001**, *115*, 2576.

(62) Dixon, D. A.; Gutowski, M. *J. Phys. Chem. A* **2005**, *109*, 5129.

(63) Grant, D.; Dixon, D. A. *J. Phys. Chem. A* **2005**, *109*, 10138.

(64) Matus, M. H.; Anderson, K. D.; Camaioni, D. M.; Autrey, S. T.; Dixon, D. A. *J. Phys. Chem. A*, WEB ASAP, April 2007.

(65) Pollack, L.; Windus, T. L.; de Jong, W. A.; Dixon, D. A. *J. Phys. Chem. A* **2005**, *109*, 6934.

(66) Frisch, M. J.; Trucks, G. W.; Schlegel, H. B.; Scuseria, G. E.; Robb, M. A.; Cheeseman, J. R.; Montgomery, J. A., Jr.; Vreven, T.; Kudin, K. N.; Burant, J. C.; Millam, J. M.; Iyengar, S. S.; Tomasi, J.; Barone, V.; Mennucci, B.; Cossi, M.; Scalmani, G.; Rega, N.; Petersson, G. A.; Nakatsuji, H.; Hada, M.; Ehara, M.; Toyota, K.; Fukuda, R.; Hasegawa, J.; Ishida, M.; Nakajima, T.; Honda, Y.; Kitao, O.; Nakai, H.; Klene, M.; Li, X.; Knox, J. E.; Hratchian, H. P.; Cross, J. B.; Bakken, V.; Adamo, C.; Jaramillo, J.; Gomperts, R.; Stratmann, R. E.; Yazyev, O.; Austin, A. J.; Cammi, R.; Pomelli, C.; Ochterski, J. W.; Ayala, P. Y.; Morokuma, K.; Voth, G. A.; Salvador, P.; Dannenberg, J. J.; Zakrzewski, V. G.; Dapprich, S.; Daniels, A. D.; Strain, M. C.; Farkas, O.; Malick, D. K.; Rabuck, A. D.; Raghavachari, K.; Foresman, J. B.; Ortiz, J. V.; Cui, Q.; Baboul, A. G.; Clifford, S.; Cioslowski, J.; Stefanov, B. B.; Liu, G.; Liashenko, A.; Piskorz, P.; Komaromi, I.; Martin, R. L.; Fox, D. J.; Keith, T.; Al-Laham, M. A.; Peng, C. Y.; Nanayakkara, A.; Challacombe, M.; Gill, P. M. W.; Johnson, B.; Chen, W.; Wong, M. W.; Gonzalez, C.; Pople, J. A. *Gaussian 03*, revision D.02; Gaussian, Inc.: Wallingford, CT, 2004.

(67) Dunlap, B. I. *J. Chem. Phys.* **1983**, *78*, 3140.

(68) Dunlap, B. I. *J. Mol. Struct. (THEOCHEM*). **2000**, *529*, 37.

(69) Werner, H.-J.; Knowles, P. J.; Lindh, R.; Manby, F. R.; Schütz, M.; Celani, P.; Korona, T.; Rauhut, G.; Amos, R. D.; Bernhardsson, A.; Berning, A.; Cooper, D. L.; Deegan, M. J. O.; Dobbyn, A. J.; Eckert, F.; Hampel C.; Hetzer, G.; Lloyd, A. W.; McNicholas, S. J.; Meyer W.; Mura, M. E.; Nicklass, A.; Palmieri, P.; Pitzer, R.; Schumann, U.; Stoll, H.; Stone, A. J.; Tarroni, R.; Thorsteinsson, T. *MOLPRO*, version 2006.1, a package of ab initio programs; see http://www.molpro.net. (September 2007).

(70) Bylaska, E. J.; de Jong, W. A.; Kowalski, K.; Straatsma, T. P.; Valiev, M.; Wang, D.; Aprà, E.; Windus, T. L.; Hirata, S.; Hackler, M. T.; Zhao, Y.; Fan, P.-D.; Harrison, R. J.; Dupuis, M.; Smith, D. M. A.; Nieplocha, J.; Tipparaju, V.; Krishnan, M.; Auer, A. A.; Nooijen, M.; Brown, E.; Cisneros, G.; Fann, G. I.; Früchtl, H.; Garza, J.; Hirao, K.; Kendall, R.; Nichols, J. A.; Tsemekhman, K.; Wolinski, K.; Anchell, J.; Bernholdt, D.; Borowski, P.; Clark, T.; Clerc, D.; Dachsel, H.; Deegan, M.; Dyall, K.; Elwood, D.; Glendening, E.; Gutowski, M.; Hess, A.; Jaffe, J.; Johnson, B.; Ju, J.; Kobayashi, R.; Kutteh, R.; Lin, Z.; Littlefield, R.; Long, X.; Meng, B.; Nakajima, T.; Niu, S.; Pollack, L.; Rosing, M.; Sandrone, G.; Stave, M.; Taylor, H.; Thomas, G.; van Lenthe, J.; Wong, A.; and Zhang, Z. *NWChem, A Computational Chemistry Package for Parallel Computers, Version 5.0* Pacific Northwest National Laboratory, Richland, WA 99352−0999, 2006.

(71) Kendall, R. A.; Aprà, E.; Bernholdt, D. E.; Bylaska, E. J.; Dupuis, M.; Fann, G. I.; Harrison, R. J.; Ju, J.; Nichols, J. A.; Nieplocha, J.; Straatsma, T. P.; Windus, T. L.; Wong, A. T. *Comput. Phys. Commun.* **2000**, *128*, 260.

(72) Deegan, M. J. O.; Knowles, P. J. *Chem. Phys. Lett.* **1994**, *227*, 321.

(73) Knowles, P. J.; Hampel, C.; Werner, H.-J. *J. Chem. Phys.* **1993**, *99*, 5219.

(74) Rittby, M.; Bartlett, R. J. *J. Phys. Chem*. **1988**, *92*, 3033.

(75) Li, S.; Clouthier, D. J. Manuscript to be published.

(76) Yang, D.-S.; Zgierski, M. Z.; Rayner, D. M.; Hackett, P. A.; Mrtinex, A.; Salahub, D. R.; Roy, P. N.; Carrington, T., Jr. *J. Chem. Phys.* **1995**, *103*, 5335.

(77) Gruner, D.; Brumer, P. *Chem. Phys. Lett.* **1987**, *138*, 310.

(78) Ruhoff, P. T.; Ratner, M. A. *Int. J. Quant. Chem.* **2000**, *77*, 383.

(79) Hazra, A.; Nooijen, M. *Int. J. Quantum Chem.* **2003**, *95*, 643.

(80) Moore, C. E. Atomic energy levels as derived from the analysis of optical spectra, Volume 1, H to V. U.S. National Bureau of Standards Circular 467; U.S. Department of Commerce, National Technical Information Service, COM-72-50282: Washington, DC, 1949.

(81) Chase, M. W., Jr. *NIST-JANAF Thermochemical Tables*, 4th ed. *J. Phys. Chem. Ref. Data* **1998**, Mono. 9, Suppl. 1.

(82) Curtiss, L. A.; Raghavachari, K.; Redfern, P. C.; Pople, J. A. *J. Chem. Phys.* **1997**, *106*, 1063.

(83) Zhai, H.-J.; Li, S.; Dixon, D.A.; Wang, L.-S. *J. Am. Chem. Soc.*, to be submitted for publication, 2007.

(84) Stolcic, D.; Kim, Y. D.; Gantefor, G. *J. Chem. Phys.* **2004**, *120*, 5.

(85) Lee, T. J.; Taylor, P. R. *Int. J. Quantum Chem.* **1989**, *S23*, 199.

(86) (a) Kowalski, K.; Piecuch, P. *J. Chem. Phys.* **2000**, *113*, 18. (b) Kowalski, K.; Piecuch, P. *J. Chem. Phys.* **2000**, *113*, 5644.

(87) Kowalski, K. *J. Chem. Phys.* **2005**, *123*, 014102.

(88) Kowalski, K.; Piecuch, P. *J. Chem. Phys.* **2005**, *122*, 074107.

(89) Rothschopf, G. K.; Perkins, J. S.; Li, S.; Yang, D.-S. *J. Phys. Chem. A* **2000**, *104*, 8178.

(90) Li, S.; Rothschopf, G. K.; Pillai, D.; Sohnlein, B. R.; Wilson, B. M.; Yang, D.-S. *J. Chem. Phys.* **2001**, *115*, 7968.

(91) Li, S.; Rothschopf, G. K.; Yang, D.-S. *J. Chem. Phys.* **2002**, *116*, 6589.

(92) Sohnlein, B. R.; Li, S.; Fuller, J. F.; Yang, D.-S. *J. Chem. Phys.* **2005**, *123*, 014318.

(93) Lau, K. C.; Kandalam, A. K.; Costales, A.; Pandey, R. *Chem. Phys. Lett.* **2004**, *393*, 112.

(94) (a) Helgaker, T.; Klopper, W.; Koch, H.; Noga, J. *J. Chem. Phys.* **1997**, *106*, 9639. (b) Halkier, A.; Helgaker, T.; Jørgensen, P.; Klopper, W.; Koch, H.; Olsen, J.; Wilson, A. K. *Chem. Phys. Lett.* **1998**, *286*, 243.

(95) (a) Feller, D. *J. Chem. Phys.* **1992**, *96*, 6104. (b) Xantheas, S. S.; Dunning, T. H.; Jr. *J. Phys. Chem*. **1993**, *97*, 18. (c) Feller, D. *J. Chem. Phys.* **1993**, *98*, 7059.

(96) Balabanov, N.B.; Peterson, K.A., *J. Chem. Phys.* **2005**, *123*, 064107.

(97) Huber, K. P.; Herzberg, G. *Molecular Spectra and Molecular Structure IV: Constants of Diatomic Molecules*; Van Nostrand Reinhold: New York, 1979.

(98) Cotton, F. A.; Wilkinson, G.; Murillo, C. A.; Bochmann, M. *Advanced Inorganic Chemistry*, 6th ed.; Wiley: New York, 1999.